UNIVERSITY OF HELSINKI
DEPARTMENT OF PHYSICS

REPORT SERIES IN GEOPHYSICS

No 73

ON OPTICAL AND PHYSICAL PROPERTIES OF SEA ICE IN THE BALTIC SEA

Cover picture:

Some fine moments of field work. Gulf of Bothnia, Baltic Sea.

Jari Uusikivi

HELSINKI 2013

Supervisors:

Prof. Matti Leppäranta
Department of Physics
Division of Geophysics and Astronomy
University of Helsinki
Helsinki, Finland

Dr. Anssi Vähätalo
Department of Environmental Sciences
University of Helsinki
Helsinki, Finland

Pre-examiners:

Prof. Timo Huttula
Finnish Environment Institute
Jyväskylä, Finland

Dr. Jari Haapala
Finnish Meteorological Institute
Helsinki, Finland

Opponent:

Prof. Peter Wadhams
University of Cambridge
Cambridge, Great Britain

Custos:

Prof. Ilmo Kukkonen
Department of Physics
Division of Geophysics and Astronomy
University of Helsinki
Helsinki, Finland

Report Series in Geophysics No. 73

ISBN 978-952-10-8097-5 (paperback)
ISSN 0355-8630
Helsinki 2013
Unigrafia

ISBN 978-952-10-8098-2 (pdf)
http://ethesis.helsinki.fi
Helsinki 2013
Helsingin yliopiston verkkojulkaisut

ON OPTICAL AND PHYSICAL PROPERTIES OF SEA ICE IN THE BALTIC SEA

Jari Uusikivi

ACADEMIC DISSERTATION IN GEOPHYSICS

To be presented, with the permission of the Faculty of Science of the University of Helsinki for public criticism in Auditorium E204 of Physicum, Gustaf Hällströmin katu 2A, on June 28th, 2013, at 12 o'clock noon.

Helsinki 2013

Contents

Abstract

Sea ice has been recognized as one of the key elements of polar and subpolar seas, including the Baltic Sea. The existence of sea-ice cover and its properties influence many aspects of marine biology, climate, and seafaring. Here, I focus on describing the physical and optical properties of landfast ice and pack ice in the Baltic Sea. The aim of the thesis is to determine the interactions between optical and physical properties of sea ice and how these can affect the biology in sea ice.

Decade-long observations of ice properties were used to construct a statistical model of the properties of landfast ice. Temperature was the most important factor in determining ice thickness, while the contribution of snow ice to the ice thickness was determined by the amount of wintertime precipitation. The stratigraphy of the ice and its growth history influenced the vertical distribution of organisms in the ice cover, because the snow ice layers and columnar ice layers favored different types of organisms. The thickness of the meteoric ice layer, including snow ice and superimposed ice, controlled the albedo of the ice cover when no snow cover was on the ice. Based on the observations of fast ice conditions and albedo, the effects of snow thickness and meteoric ice thickness on the albedo of sea ice were formulated as albedo parameterization equations.

The optical properties of sea ice with spectral resolution were studied on landfast sea ice. Emphasis in these studies was given to optical properties in the ultraviolet (UV) and visible wavelengths. Organic matter, dissolved and particulate, was the most important factor determining the UV properties of the sea-ice cover. The optical properties in the UV were also actively modified by the living organisms in the ice cover by producing mycosporine like amino acids (MAAs) in relatively high amounts. MAAs are a family of photoprotective compounds that absorb UV radiation efficiently. In the visible part of the spectrum, the ice by itself and the thickness of meteoric ice layer were the most important determinants.

Salinity and the initial salt entrapment during ice growth in the Baltic Sea were less than in the oceans with equal ice growth rates. The turbulent fluxes of heat and salinity under the landfast sea ice were small.

List of original publications

This thesis is based on the following articles and referred to by their Roman numerals:

I. Uusikivi, Jari, Mats A. Granskog and Eloni Sonninen. 2011. Meteoric ice contribution and influence of weather on landfast ice growth in the Gulf of Finland, Baltic Sea. Annals of Glaciology 52(57): 91-96.

II. Uusikivi, Jari, Anssi V. Vähätalo, Mats A. Granskog and Ruben Sommaruga. 2010. Contribution of mycosporine-like amino acids and colored dissolved and particulate matter to sea ice optical properties and ultraviolet attenuation. Limnoly & Oceanography 55: 703-713.

III. Uusikivi, Jari, Jens Ehn and Mats A. Granskog. 2006. Direct measurements of turbulent momentum, heat and salt fluxes under landfast ice in the Baltic Sea. Annals of Glaciology 44: 42-46.

IV. Rintala, Janne-Markus, Jonna Piiparinen and Jari Uusikivi. 2009. Drift-ice and under-ice water communities in the Gulf of Bothnia (Baltic Sea). Polar Biology 33(2):179-191, DOI 10.1007/s00300-009-0695-1

V. Granskog, Mats A., Jari Uusikivi, Alberto Blanco Sequeiros and Eloni Sonninen. 2006. Relation of ice growth rate to salt segregation during freezing of low-salinity seawater (Baltic Sea). Annals of Glaciology 44: 134-138.

VI. Uusikivi, Jari and Kunio Shirasawa. Seasonal evolution of albedo in the landfast sea ice. (manuscript, submitted to Boreal Environment Research on 16.1.2013)

The author's own contribution to each publication in percentage of the workload (1 < 20%, 2 20-70% and 3 > 70%) and classified as idea, practical work (including sample collection, preparation, and analytical work), and writing (including data analysis and manuscript preparation):

Article	Idea	Practical work	Writing
I	3	2	3
II	2	2	3
III	2	2	3
IV	1	1	1
V	1	2	1
VI	3	2	3

1 Introduction

Sea ice greatly influences many aspects of marine biology, climate, and seafaring. Although Baltic Sea ice has been the focus of quite a variety of research (see Leppäranta et al. 2001), the basic importance of the annual ice cover is not well known, especially for the environment and ecosystems (Granskog et al. 2010). Baltic Sea ice studies have long been focused on the ice extent and large-scale ice thicknesses that have been needed for producing sea-ice maps for winter navigation. There are long observation datasets from the Baltic Sea on the maximum sea-ice extent (since the 16th century) and maximum ice thickness (since 1899) (Vihma and Haapala 2009).

The first studies to address the structure and small-scale properties of landfast ice in the Baltic Sea were carried out by E. Palosuo in the 1950s (Palosuo 1961; 1963). Since then, for decades the focus in Baltic Sea ice research has been directed towards large-scale properties and dynamics of sea ice (see Vihma and Haapala 2009). There have been only a few notable exceptions to this trend before the turn of the last century, such as the studies by Omstedt (1985) on the crystal structures of ice, Leppäranta and Manninen (1988) on ice salinity, and Weeks et al. (1990) on the structure and composition of landfast ice. Meanwhile the large- and small-scale properties of oceanic (water salinity > 24.7 practical salinity units (psu)) sea ice have been the focus of quite a variety of research efforts, starting from Malgrens doctoral thesis in 1927 (Weeks 1998) to thorough reviews of the properties and processes by Weeks and Ackley (1982) and Petrich and Eicken (2010). The fast ice of the Baltic Sea and more detailed study of the salinity, albedo, and the distribution, size, and morphology of ice crystals and inclusions, as well as meteoric ice contribution, became subjects of increased focus after the Finnish-Japanese cooperative program was initiated in 1998 (Kawamura et al. 2001; Granskog et al. 2004). This was soon followed by the first detailed optical studies of Baltic Sea ice (Rasmus et al. 2002; Ehn et al. 2004), published almost three decades after the first comprehensive optical studies from the Arctic Ocean (Maykut and Grenfell 1975). Ehn et al. (2004) were also the first to study the effects of the high amounts of particulate and dissolved organic matter on the optical properties of the Baltic Sea ice.

The first records of the biology in sea ice were published in 1841 by C. G. Ehrenberg (Dieckmann and Hellmer 2010), after which further articles followed on the subject. Over the past 50 years, the efforts to study sea-ice ecology in polar oceans have been numerous and manifold (Mock and Thomas 2005). The biological studies of Baltic Sea ice are quite a newer addition to the scientific discussion, with the first results from the 1980s and more systematic research after the mid-1990s (Granskog et al. 2006b). Ice biology is in many ways influenced by the physical properties of sea ice; e.g. algae experience a more steady growth environment inside the ice than in the open sea, although the light, salinity, and temperature conditions are drastically different. In the pursuit to understand sea ice as a whole, it is quite a natural continuum to combine the various disciplines of ice research and join forces to create a more multidisciplinary approach. This type of new approach began to emerge in the late 1990s and has since produced advances in ice research (Mock and Thomas 2005). The studies of Baltic Sea ice have been in the forefront of this type of multidisciplinary research (Granskog et al. 2006b), despite lacking in many aspects of more traditional ice research.

Sea ice is also an important factor in future climate conditions. Climate is in many ways influenced by the presence or absence of ice cover (Rind et al. 1995; Holland and Bitz 2003). High sea-surface albedo, in contrast to the much lower open-water albedo, greatly affects radiative forcing at the surface. The sea-ice albedo climate feedback mechanism is the most important factor in considering sea-ice covers (Holland et al. 2001) and surface albedo and input of solar radiation to the ocean are

major constituents of this mechanism (Curry et al. 1995). The ice cover also drastically influences air-sea exchange of energy, momentum and gases.

1.1 Goals of this work

The aim of this thesis is to increase our understanding of sea-ice properties, optics, and interaction between the physical properties of ice with biology and biogeochemistry, especially in the fast ice areas of the Baltic Sea. The objectives can be divided into two fundamental themes. The first is an attempt to formulate the sea-ice salinity characteristics of the Baltic Sea. To do this some background data on the salinity fluxes between ice and water and salt segregation into the ice were needed. These processes are crucial to an understanding of sea-ice salinity and possible exchange between brine pockets and under-ice water. The second objective is to define the most important factors affecting sea-ice optical properties, both from the energy budget and ecology perspectives. The optical properties are largely dependent on sea-ice structure and stratigraphy. The objective was to link these properties and formulate a parameterization for possible model applications. Furthermore, if one wants to understand the seasonal, interannual, and temporal changes in optical properties, an understanding of variations in the ice structure are of great importance. Therefore, spatial and temporal variation studies of sea-ice structure and stratigraphy were also carried out.

The albedo and transmittance of light are the most covered optical properties of sea ice and are also the most common properties related to biology and the environment. Surface layers that have a white appearance to them, such as snow and superimposed ice layers, greatly affect the albedo and optical properties of the ice cover (Light et al. 2008). Gas inclusions (e.g. air bubbles) are typically concentrated in the surface-scattering layer and are incorporated in the ice cover through snow ice formation or melting and refreezing of the ice surface. Snow ice layers are typical of the Baltic Sea ice cover and their contribution to the ice thickness was first reported by Palosuo (1963). Later studies confirmed the large contribution of snow and superimposed ice to Baltic Sea ice. Depending on the season and year, meteoric ice (snow and superimposed ice combined) may contribute almost half of the total thickness and up to 35% of the total mass of landfast ice (Granskog et al. 2003; 2004). We examined sea-ice growth, structure, and salinity in the Baltic Sea (I, III-V). These studies also included efforts to relate ice biology to ice structure and associate the ice growth processes to the environmental conditions.

The transmittance of solar radiation through ice is an important factor affecting biological activity in and under sea ice (Perovich et al. 1993; Perovich 2003). The most important factors controlling the transmission of light through a sea-ice cover are the ice itself, gas and brine inclusions, particulate matter (PM), and colored (also called chromophoric) dissolved organic matter (CDOM) incorporated into the ice cover (Perovich et al. 1998; Belzile et al. 2000). Photosynthetically active radiation (PAR, 400-700 nm) drives photosynthesis, while ultraviolet (UV) radiation (280-400 nm) has many direct and indirect harmful effects on biota. Therefore, it is equally important to understand the penetration of both PAR and UV radiation through the ice (Perovich et al. 1993). The contribution of CDOM and PM to the optical properties of sea ice and to the attenuation of UV radiation in sea ice is not well understood (Belzile et al. 2000). Further knowledge on this topic is needed because previous studies indicated that ice algae adapted to the low-light conditions prevailing under snow and ice covers are potentially sensitive to UV radiation (Cota et al. 1991; Prezelin et al. 1998). In this context, CDOM can be both a shield from harmful UVR and a potential precursor for biologically labile compounds that could enhance biological activity; however, the overall effect on sea-ice communities is not well understood.

We focused on the radiative transfer of sea ice, including the albedo of sea ice, absorption of light, transmittance, and light intensities inside the ice cover, as well as ice stratigraphy and growth history as related to the optical properties of ice (II,VI), findings associated with those found elsewhere (I, III-V).

The results presented here covered many ice properties and advanced the understanding of various processes associated with to sea ice, and are further detailed in Figure 1 and the following chapters. These chapters begin at the smallest and progress towards larger scales.

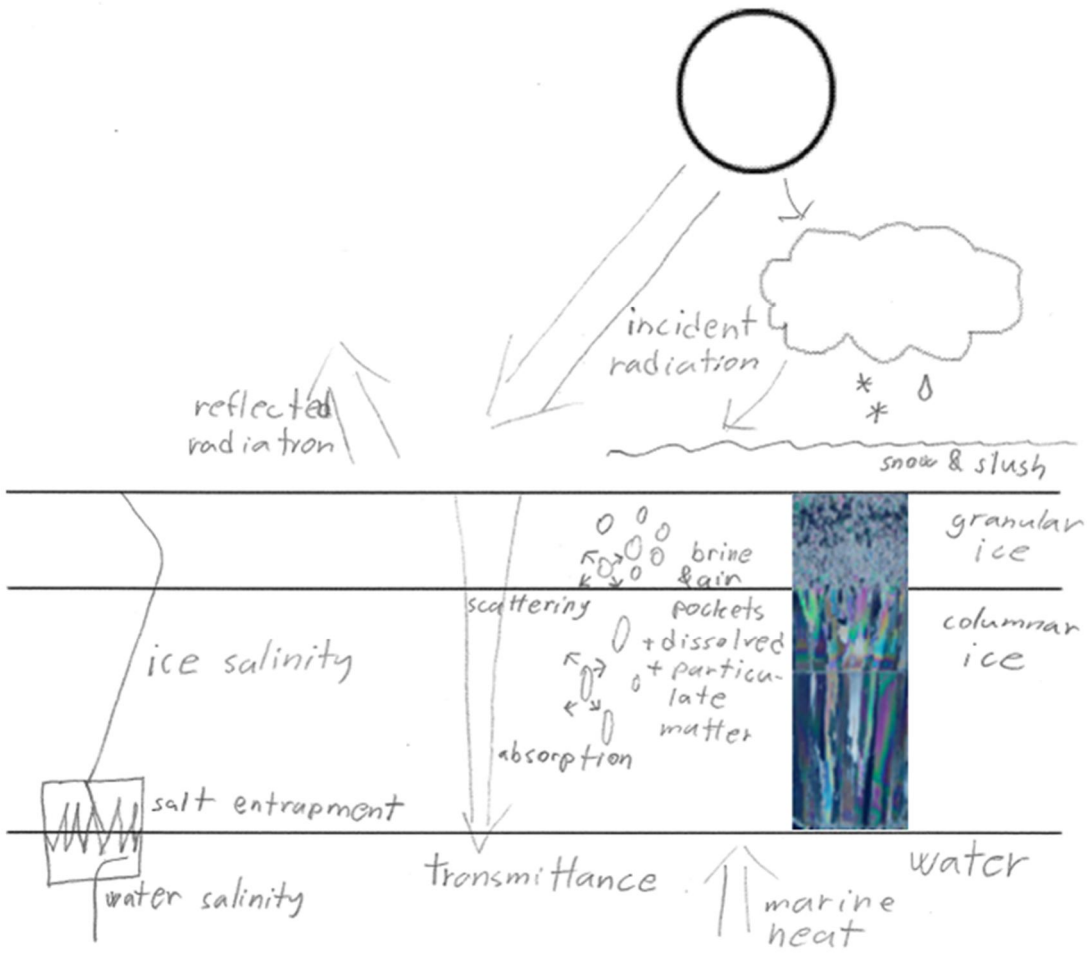

Figure 1. Schematic figure of the sea-ice-related processes and properties covered in this thesis. Further details are provided in the following chapters.

2 Baltic Sea characteristics and measurement sites

The Baltic Sea is a small intracontinental arm of the Atlantic Ocean and is the second largest brackish water (water salinity less than 24.7 psu and more than 0.5 psu) basin in the world, with a mean salinity of about 7 psu. The brackish water is a result of isolation from the saline waters of the Atlantic Ocean due to the rather narrow and shallow Danish Straits and strongly positive freshwater budget due to river discharge. The low salinity of the brackish water in the Baltic Sea means that the freezing point of water is just slightly below 0 ºC and the temperature of maximum density is between 2 ºC and 3 ºC (Leppäranta and Myrberg 2009). The Baltic Sea is considerably smaller than the Arctic Ocean or North Sea, with an area of 393 000 km^2 and mean depth of 54 m (Leppäranta and Myrberg 2009). The Baltic Sea basin has three major gulfs in its northern and eastern parts; the gulfs of Bothnia, Finland, and Riga. These gulfs have lower water salinities in the surface layers than the rest of the Baltic Sea and are also more likely to be covered with ice during winter.

On the coasts of Finland and Sweden in the Gulf of Bothnia, the sea is generally ice-covered between 2 and 7 months, typically between December and March. The ice conditions in the Baltic Sea can be characterized by the large interannual variability in the extent of ice cover; 10-100% of the surface area is ice-covered, depending on the severity of the winter (Granskog et al. 2010). The average ice-cover season length is 6.4 months and average maximum annual ice extent 45% of the Baltic Sea area (Leppäranta and Myrberg 2009). The ice regime in the Baltic Sea can be divided into landfast ice cover along the coasts and mobile pack ice further offshore. The many islands and islets bordering the coasts in the northern Baltic increase the extent of landfast ice cover, which is anchored to them and so wind breakup does not often occur. On average, the boundary between the fast ice and pack ice regimes follows the 10-m isobath (Leppäranta 1981). The thickest fast ice measured in the Baltic Sea was 1.22 m, measured in Tornio during the winter of 1985 (Leppäranta and Myrberg 2009).

Regardless of the distinct differences between the Arctic or Antarctic Oceans and the Baltic Sea, the ice covers in all these areas show many similarities. The most pertinent may be that despite the low water and ice salinities, the ice shows a characteristic sea-ice structure with brine inclusions (Kawamura et al. 2001) and hosts an actively functioning food web (Kaartokallio, 2004), as do its oceanic counterparts.

2.1 Study sites

All the studies presented in this thesis were carried out in two general areas of the Baltic Sea, the Gulf of Finland and the Gulf of Bothnia (Figure 2). Most of the studies focused on to the vicinity of the Hanko Peninsula on the southern coast of Finland (Figure 2, location 1) and especially in Santala Bay (Figure 2, location 1A), a semienclosed bay sheltered from the open sea by a peninsula and islands, thereby allowing fast ice to form there almost every winter. Between 1999 and 2010, only one winter was without a permanent ice cover (I). Santala Bay also has strong water exchange with adjacent sea areas and lacks any significant freshwater input, hence has water salinities similar to those of the main Baltic Sea proper. Studies in the Gulf of Bothnia were carried out in both fast ice and pack ice areas. Locations 2 and 3 in Figure 2 were fast ice sites and locations a-f pack ice sites.

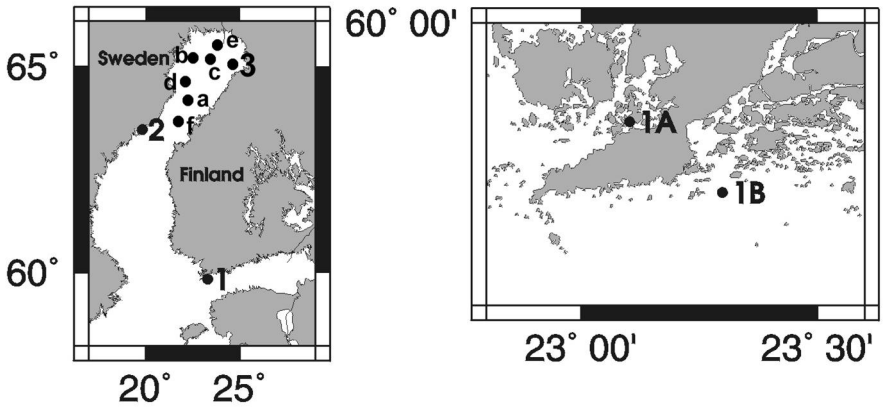

Figure 2. Study locations between 1999 and 2009. The map on the right is a close-up of location 1 on left. Turbulence studies (III) were conducted at locations 1A, 1B, and 2, salt segregation studies (V) at 3, optical studies (II and VI) at 1A, pack ice studies (IV and other pack ice studies in 2007 and 2009) at locations a-f, and ice stratigraphy and weather studies (I) at 1A.

3 Methods and field data

3.1 Ice texture, growth history, and salinity analysis

Sea-ice crystal texture can be studied, using thin sections of ice viewed by eye between crossed polarizing plates (see Figures 3a and 3b). Growth history and growth processes can be studied, using a stable oxygen isotope ($\delta^{18}O$) ratios, which is a ratio of two stable oxygen isotopes (^{18}O:^{16}O) in the sample and its relative deviation from the isotope ratio of the international reference Vienna Standard Mean Ocean Water (VSMOW).

The isotope ratio is different in the ocean and atmosphere, since there is a difference in the volatility of these two isotopes. The atmospheric values vary due to the temperature and humidity of the air mass, which affects the volatility of the isotopes. In a simplified concept, $\delta^{18}O$ is closer to zero the longer that water molecule have been in the liquid state, i.e. $\delta^{18}O$ in freshwater lakes and rivers is less negative than that in rainwater and more negative than that in the Baltic Sea. The $\delta^{18}O$ values vary from 0 ‰ for ocean water to -8 ‰ for Santala Bay water and for -17 ‰ fresh snow, but the snow values especially can vary substantially. Using these differences in $\delta^{18}O$ values together with ice structure, one can track the origin of the water in the sample and in the case of sea ice the fraction of meteoric ice in the sample. Granular ice structures with $\delta^{18}O$ values close to those of snow and lower than those of the parent seawater indicate meteoric ice layers. Frazil ice also has a granular ice structure, but has $\delta^{18}O$ values higher than or equal to those of the parent seawater. For columnar ice, the $\delta^{18}O$ values are higher than the parent seawater values as a result of isotopic fractionation during freezing, when freezing of seawater excludes more of the light isotopes than the heavy isotopes. This fractionation is also ice growth velocity-dependent and becomes larger the more slowly that ice grows (Tison et al. 2001).

The $\delta^{18}O$ data of melted ice samples were used to determine the fraction of precipitation in the snow ice and superimposed ice layers, and in the total ice thickness. The fraction of precipitation in the ice layers was based on calculating the snow fraction (f_s) from the $\delta^{18}O$ data (Lange et al. 1990; Jeffries et al. 1994):

$$f_s + f_{sw} = 1 \quad (1)$$

$$f_s \delta_s + f_{sw} \delta_{sw} = \delta \quad (2)$$

where f_{sw} is the seawater fraction of the sample, δ_s and δ_{sw} are the $\delta^{18}O$ values of snow and seawater, respectively, and δ is the $\delta^{18}O$ value of the sample. Granular ice classification into snow ice and superimposed ice is based on f_s values, according to Granskog et al. (2004). The superimposed ice layers were identified as those with $f_s \geq 0.65$. Snow ice layers were identified as those with $0.65 > f_s \geq 0$.

3.2 Under-ice turbulence

Measurements of under-ice turbulence in this study were performed, using an acoustic Doppler 3D current meter (Vector; Nortek AS, Rud, Norway) with an attached fast repetition temperature-conductivity sensor (Accurate Conductivity Temperature meter, PME, California, USA). The measurement accuracy of the current meter was ±1 mm s^{-1}, with a sampling volume of 884 mm^3 (diameter 15 mm, height 5 mm). The accuracy of the conductivity measurements was 0.1% and

temperature measurement accuracy 0.020 ºC. The sensors were deployed either through the ice to the underlying water column while suspended by a fiberglass shaft from the ice or mounted directly on the ice cover with the access hole insulated to prevent freezing in the hole. The measurement depths varied between 0.22 m and 3 m beneath the ice bottom, with the majority of the measurements done between 0.22 m and 1.35 m below the ice bottom. The measurement periods ranged from 20 minutes to three days per location. Eddy correlation techniques were applied and the values for heat and salinity flux, friction velocity, roughness Reynolds number and heat transfer coefficient were calculated. All measurements were checked for quality and divided into 10-minute periods, while periods with more than 30 % of substandard data were omitted from analysis.

The flow in the under-ice water surface layer consisted of three types of flow regimes, i.e. laminar flow close to the ice-water boundary, transitional flow between the other two flow regimes, and a turbulent-flow regime furthest away from the boundary. The Reynolds number (Re) and roughness Reynolds number (Re_*) are used to determine the current flow regime and whether the flow is hydrodynamically rough or smooth. Re and Re_* are defined as (Shirasawa and Ingram 1991a; 1991b):

$$\mathrm{Re} = \frac{UD}{\nu} \tag{3}$$

$$\mathrm{Re}_* = \frac{30 u_* z_0}{\nu} \tag{4}$$

where U is the current velocity, D is the distance from the ice bottom, ν is the kinematic viscosity of seawater, u_* is the friction velocity, and z_0 is the roughness length, $z_0 = 30\ k_s$, where k_s is the mean height of the roughness elements.

In the turbulent-flow regime the turbulent flux quantities can be obtained as deviations from an average, e.g. $T' = T - \langle T \rangle$. T is the temperature measured and ‹ › denotes an average value. Using the formulation of McPhee (1992; 2002), momentum τ, oceanicheat F_w and salinity S_w fluxes, and friction velocity u_* can be calculated with the following equations:

$$\tau = \left(\langle u'w' \rangle^2 + \langle v'w' \rangle^2 \right)^{1/2} \tag{5}$$

$$u_* = |\tau|^{1/2} \tag{6}$$

$$F_w = \rho_w c_p \langle w'T' \rangle \tag{7}$$

$$S_w = \langle w'S' \rangle \tag{8}$$

where ρ_w is the seawater density, u′ is the east deviation velocity, v′ is the north deviation velocity, w′ is the vertical deviation velocity, c_p is the specific heat of seawater, T′ is the seawater deviation temperature, and S′ is the seawater deviation salinity.

3.3 Optical measurements

The optical properties of sea ice were covered in two studies in the thesis, both of which were conducted in Santala Bay (location 1A in Figure 2). We measured the apparent optical properties (AOPs) with three Ramses-ACC VIS hyperspectral radiometers (TriOS Optical Sensors, Germany) (II). These sensors measured upwelling or downwelling plane irradiances, using a cosine collector in the wavelength range from 320 nm to 950 nm and sampling bandwidth of 3.3 nm. To measure the transmitted irradiances, an aluminum arm with floats was used to position the sensors under the ice. The arm was installed through a 30 cm x 30 cm hole in the ice and the sensors were positioned 3 cm below the ice bottom, 1 m south of the hole. A Macam SR991 spectroradiometer (Macam Photometrics, UK) equipped with a cosine collector attached to a 4.2 m long optical fiber was used to measure the irradiances between 305 nm and 400 nm with a 2-nm bandwidth at 5 nm intervals. In this case, a single instrument was used to make successive measurements of incident, reflected, and transmitted irradiances. Irradiance attenuation in the interior of the ice was measured with an inverted Ramses radiometer, following the method described by Grenfell et al. (2006). In this setup, the sensor was mounted on a 5 cm diameter metal housing pointing downwards to a diffuse reflector surface and then inserted into a 5.2 cm diameter hole that was drilled through the ice and set to different depths at 5 cm intervals.

The spectral absorption coefficients of colored dissolved organic matter (a_{CDOM}) and particulate matter (a_{p}) were measured in the laboratory at the Tvärminne Zoological Station from melted ice core samples. The water from the melted ice cores was filtered through fiberglass filters (Whatman GF/F 25-mm diameter, nominal pore size of 0.7μm) in an all-glass filtration device (19-mm diameter of the filtering area) with low vacuum. The filtrate was collected for a_{CDOM} measurements. The filters were placed into small dishes, kept in darkness, and a_{p} was measured within a few hours or from frozen (-18°C) filters on the next day. The CDOM spectra were measured against Milli-Q blanks from 200 nm to 800 nm with 2-nm slits and at 1-nm intervals, using a Shimadzu UV-2501 PC spectrophotometer (Shimadzu). The a_{p} was measured with an ISR-240A integrating sphere (Shimadzu) by the 'transmittance-reflectance' method (Tassan and Ferrari 2002), using a quartz support that allowed measurements also in the UV region. The scattering coefficients were not measured, but calculated using Equation 14, with the downwelling irradiance (K_d) and total absorption coefficient of the sea ice (a_{tot}) measured.

The albedo measurements were taken with an automatic station set on a float in Santala Bay before winter freeze-up and subsequently frozen to the ice cover during the winter in 2000 and 2001 (VI). The station recorded incident and reflected radiation and surface brightness temperature, together with wind and air temperature at 1 hour intervals. The incident and reflected radiations were integrated over the time period when the sun was more than 5 degrees above the horizon and were used to calculate daily average albedos. We used the daily average albedos to minimize the effect of solar zenith angle changes, since the surface and ice conditions were available as daily averages only.

4 Sea-ice growth and microstructure

The initial growth of sea ice from seawater occurs by incorporating water molecules into a grid structure. Depending on the water surface conditions and ice growth velocity, this can result in two distinctly different crystal structures, columnar or granular. Columnar crystals are vertically elongated and can grow to several centimeters in diameter and tens of centimeters in length. A granular structure is composed of isomeric or prismatic crystals from a few to several tens of millimeters in diameter. After initial ice formation, sea ice can grow either from the top or bottom through thermodynamic processes, forming granular or columnar ice, respectively.

When ice grows through its interface with the water (i.e. the bottom), it incorporates new water molecules into the grid of molecules, forming the ice crystal. The ice crystal rejects impurities, such as salt and particles, in the water, preferring to form ice of water molecules only. However, this does not occur completely and some salt (and other impurities) are trapped in brine pockets within the growing ice sheet. These impurities impair ice-crystal growth and brine concentrates into the boundaries between the ice crystals.

Although the salinity of the Baltic Sea surface water along the coast of Finland is normally between 2 and 6 psu, the ice cover typically shows sea-ice like features, such as brine pockets and irregular crystal boundaries (Kawamura et al. 2001). At water salinities higher than about 0.6 psu, the ice formed has sea-ice characteristics, and therefore it is only in the proximity of river estuaries that Baltic Sea ice is directly comparable with freshwater ice (Palosuo 1961).

4.1 Columnar and transitional ice

Ice growth from the bottom occurs by congelation of ice crystals directly from seawater to the bottom of the ice. Under tranquil conditions, this results in a columnar ice structure (vertically elongated ice crystals, Figure 3a). When the velocity of ice growth is fast or the water under the ice is turbulent, intermediate granular/columnar (g/c) ice forms (vertically slightly elongated crystals, with grains indented and interlocked, Figure 3b) (Eicken and Lange 1989). The velocity of congelation ice growth is controlled by the heat fluxes at the top and bottom of the ice cover and the thermal properties of the ice cover. Intermediate g/c ice usually has higher average brine volume than columnar ice (IV), because there is more brine trapped in the ice. This results from a higher amount of crystal boundaries, due to smaller crystal size and typically faster growth velocity.

We concluded that the crystal structure of congelation ice, columnar or g/c, was predominantly determined by the growth velocity of ice (I). This was supported by the differences in the $\delta^{18}O$ between intermediate g/c and columnar ice. The g/c had more negative $\delta^{18}O$ values (-6.4 ‰) than columnar ice (-5.9 ‰), indicative of more rapid ice growth.

4.2 Granular ice

Granular sea ice can be of two very different genetic ice classes: meteoric or frazil ice (Haas et al. 2001) (Figures 3a and 3b). Snow ice and superimposed ice layers accumulate at the sea-ice surface and are referred to as meteoric ice because of the role of snow and rain in their formation. The texture of snow and superimposed ice is composed of orbicular and polygonal crystals, respectively (Eicken and Lange 1989; Haas et al. 2001) (Figures 3a and 3b). Snow ice is a mixture of snow and seawater that floods on ice when the mass of the snow cover is sufficient to submerge the surface of

the ice. The bottom of the snow cover is then flooded with seawater and the ensuing slush layer freezes from the top down to become an integral part of the ice cover (Weeks and Ackley 1982). The growth of snow ice is controlled mainly by the accumulation of snow on the surface of the ice, because its weight triggers the flooding and the secondary process of freezing is controlled by the air temperature and thermal properties of the snow and ice covers. Superimposed ice is completely or mainly composed of snowmelt water and/or rain that soaks the bottom layers of the snow cover and then freezes to form ice layers at the snow ice interface (Haas et al. 2001).

In addition to their appearance, snow and superimposed ice can also be distinguished, using $\delta^{18}O$ analysis. The same method can also be used to evaluate the amount of snow or rain contributing to the growth of snow ice layers, i.e. the snow fraction (f_s) using equations 1 and 2 (Lange et al. 1990; Jeffries et al. 1994). Using this method, we estimated that superimposed ice had f_s value over 0.65 and snow ice an average of 0.33 ± 0.18 (standard deviation) (I).

Frazil ice is formed primarily through the consolidation of suspended crystals in the upper part of the water column as the first form of sea ice to be seen when conditions are not totally calm (Weeks and Ackley 1982). Under quiet conditions, thin skims of ice crystals quickly consolidate and form a thin continuous ice cover that continues to grow as congelation ice. Turbulent conditions in the upper part of the water column lead to the formation of pancake ice. Pancake ice consolidates and continues growth as congelation ice after surface conditions become more tranquil. These pancake ice layers can reach thicknesses up to 0.3 m. Frazil ice layers can be recognized as layers with small orbicular crystals (Figure 3b). The $\delta^{18}O$ can be used to distinguish frazil ice from other granular ice layers, since it has no contribution from meteoric ice and the $\delta^{18}O$ values are similar to that of congelation ice and more positive than the snow and superimposed ice values.

4.3 Baltic Sea ice characteristics

Granular surface ice layers, composed of snow ice and superimposed ice, usually contribute up to half of the total landfast ice thickness in the Baltic Sea (Kawamura et al. 2001; Granskog et al. 2004), but congelation ice growth is the predominant ice growth mode. Depending on the season and year, meteoric ice may contribute almost half of the total thickness and up to 35% of the total mass of landfast ice (Palosuo 1963; Granskog et al. 2003; 2004). On landfast ice, snow ice formation is typically more important than superimposed ice formation, but superimposed ice layers can grow up to 0.10–0.15 m thick and during spring the entire snow cover can be transformed into a superimposed ice layer (Granskog et al. 2006a). Superimposed ice formation appears to be a more important contributor to ice growth in the Gulf of Bothnia than in the Gulf of Finland region (Granskog et al. 2003; 2004). Frazil ice formation has been observed in the Baltic Sea, but no previous studies or reports have quantified its contribution to the thickness of ice in the Baltic Sea.

The general contribution of different types of ice to Gulf of Finland fast ice was determined, based on a decade-long observation series (I). The columnar ice contribution to the total ice thickness ranged from 24% to 96%, with an average of 71.5 ± 21.5% (mean ± standard deviation). When present, g/c ice contributed from 11.5% to 54.5%, with an average of 23.0 ± 21.1% to the thickness of the ice. The meteoric ice contribution to the total ice thickness was from 3.7% to 38.5% with an average of 19.3 ± 11.1%. This is in good agreement with the overall contribution of meteoric ice to the ice mass along the coast of Finland, since Grankog et al. (2003) reported an 18-21% contribution of meteoric ice to the total ice mass from various measurement sites along coast.

The contribution of meteoric ice (snow and superimposed ice) to the ice thickness is equally as or more important to fast ice growth in the Baltic Sea (Kawamura et al. 2001; Granskog et al. 2003; 2004) than in the Arctic Ocean (Gow et al. 1987) and the Okhotsk Sea (Toyota et al. 2004). On the other hand, meteoric ice is not as significant a factor in the Baltic Sea as in the areas surrounding Antarctica (Jeffries et al. 1997).

Combined ice structure and biological analysis revealed that snow ice formation also influenced the vertical distribution of marine organisms and nutrients in the ice cover (IV). Snow ice layers have higher brine volume and more nutrients than columnar and g/c ice layers, because fresh seawater is incorporated directly into the ice surface layers. These highly saline and nutrient-rich ice layers have higher biomass than the ice layers below, because these layers have increased habitable space containing more nutrients and light (IV; Piiparinen et al. 2010). Increased habitable space also favors certain types of organisms (e.g. centric diatoms). Intermediate g/c ice also had higher algal biomass than columnar ice layers under similar conditions and equally thick ice covers. This was most likely due to the higher brine volumes in g/c ice and thus larger habitable space in the ice (IV). The significance of increase in habitable space is emphasized in the Baltic Sea, where low salinity sets stricter size limits for organisms than in oceanic waters (Piiparinen 2011).

4.3.1 Gulf of Bothnia pack ice properties

We examined the properties of the Gulf of Bothnia pack ice (IV), and further during March 2007 and March 2009. Pack ice is a field of ice composed of many floes that are not frozen fast to the coastline. In contrast to landfast ice, which is immobile, pack ice is in motion, driven by sea currents and winds and undergoes dynamic processes (WMO 1970). Measurements from the pack ice region revealed that frazil ice formation can be an important contributor to ice cover thicknesses (Table 1), compared with fast ice regions of the Baltic Sea where it does not contribute. These observations confirmed for the first time the common assumption that frazil ice growth contributes in some measure to the ice thickness in the Baltic Sea. Frazil ice contributed significantly (average 12.5% of thickness) to the deformed ice, which was typically composed of rafted ice floes resulting from dynamic ice processes. Generally, frazil ice contributed only marginally to the drift ice thickness (average 4.2% of thickness). The frazil ice contribution observed was quite small compared with that in the Arctic Sea (15%, Gow et al. 1987), Antarctic Ocean (44%, Jeffries et al. 1997) and Okhotsk Sea (64%, Toyota et al. 2004). In the rafted ice, congelation ice contributed 67.9% and snow ice 18% to the ice thicknesses.

Table 1. Thicknesses and mean contribution of different types of ice to the total ice thickness in different types of pack ice in the Bay of Bothnia. New ice represents refrozen leads, rafted ice is ice in which the granular ice layer is sandwiched between columnar or g/c ice layers. The table presents results (IV), supplemented with measurements from the same area in March 2007 and March 2009.

	Ice thickness (cm)			Snow ice (%)	Superimposed ice (%)	Frazil ice (%)	Congelation ice (%)	N
	Min	Max	Average					
New ice	9	33	26	17	0	2	81	4
Level ice	9	45	29	8	1	0	91	6
Rafted ice	23	58	40	18	2	13	67	5

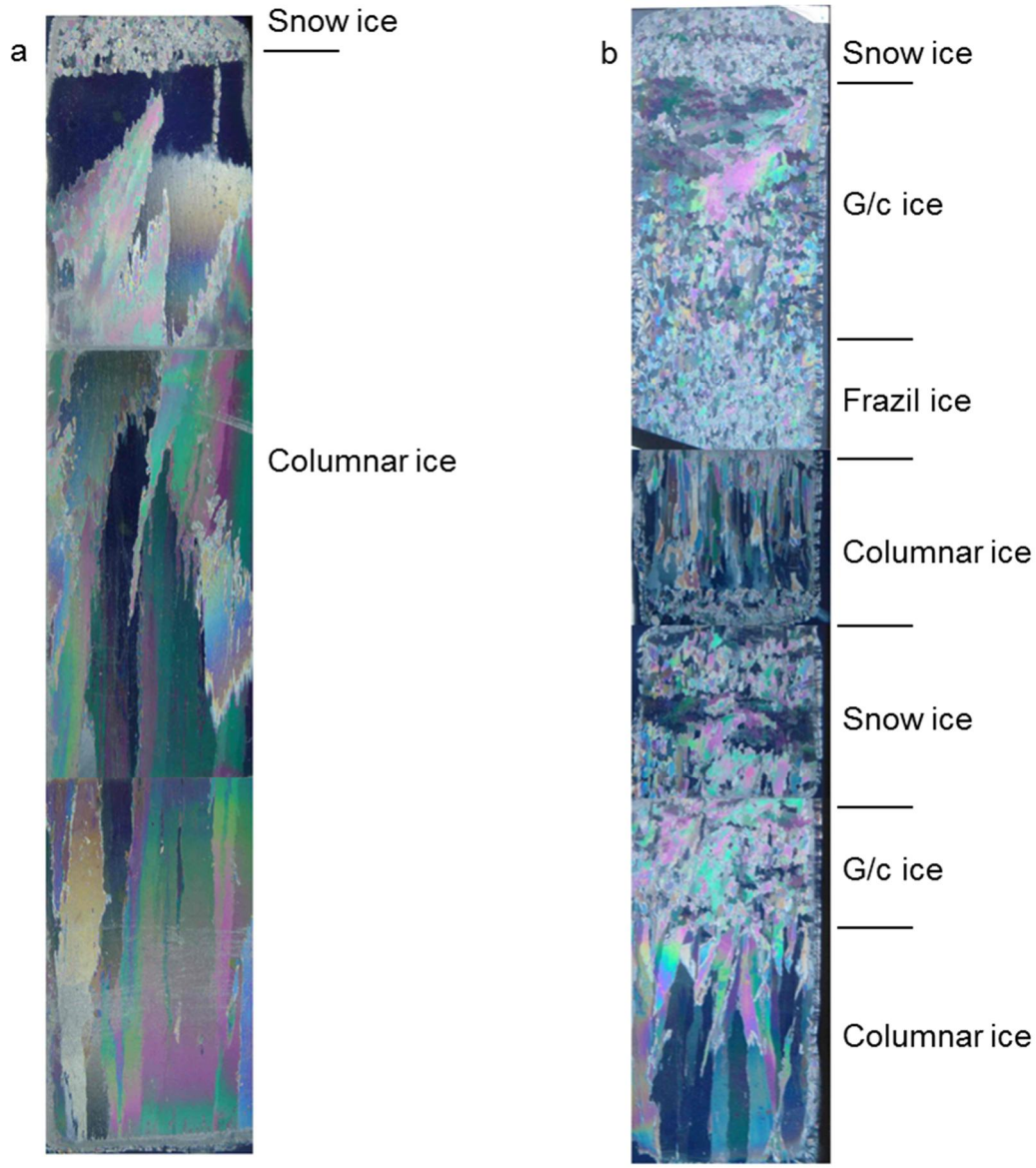

Figure 3. (a) Thin section of ice core from landfast ice in Santala Bay March 10, 2006, location 1A in Figure 2. Length of the ice core in the picture is 40.8 cm. (b) Thin section of pack ice from the Gulf of Bothnia March 4, 2006, location b in Figure 2. The ice core is 53.3 cm in length, and consists of multiple layers.

5 Ice salinity

It has long been known that sea ice contains saline brine in its pores and fluid inclusions; e.g. Mamlgren described the effects of seawater trapped in the ice in 1927 (Hobbs 1974; Feltham et al. 2006). Therefore, sea ice is also called a mushy layer, a two-phase, two-component, reactive porous medium. The mushy layer model formulates the independent, but coupled, role of two thermodynamic variables: salinity within the sea ice and temperature (Feltham et al. 2006).

The amount of brine entrapped in the ice is related to the microstructure of sea ice (i.e. the size and orientation of ice crystals) and is dependent on the rejection and entrapment processes at the growing ice-water interface. The rejection of salt results from two to three orders of magnitude slower diffusion of solute (salt) than the diffusion of heat at the water-ice boundary. During the growth of congelation ice, the advancing bottom of the ice rejects part of the salt in the water and the salinity of the ice is 5-50% of the parent seawater salinity (Weeks and Ackley 1982; Eicken 1998). The initial entrapment of salt in sea ice can be described with the salt segregation coefficient (k) (Weeks and Ackley 1982)

$$k = \frac{k_0}{k_0+(1-k_0)exp\left[\frac{\delta v}{D}\right]} \qquad (9)$$

where $k = S_i/S_w$ and S_i and S_w are the salinities of ice and water at the ice-water interface of growing ice, respectively. In sea ice, k_0 is considered to be the value of k at $v = 0$, v is ice growth velocity at the ice-water interface, δ is a measure of the boundary-layer thickness, and D is an effective transfer coefficient. The amount of salt entrapment in sea ice is then directly proportional to S_w.

After the initial formation of ice and salt entrapment, the salinity can change, especially when ice does not significantly grow or it warms to melting temperature. The most common processes that determine the later evolution of the salinity profile in the ice are brine pocket migration, brine expulsion, gravity drainage and flushing (Weeks and Ackley 1982). The sea-ice salinities of the Baltic Sea can show significant temporal fluctuations due to mild climate conditions (Granskog et al. 2004), in which flushing and gravity drainage are important processes.

Bulk salinity describes the salinity of ice in a volume, including pure ice, brine pockets, and channels. Salinity is strongly dependent on ambient water salinity and thus Baltic Sea ice reflects the low salinities of the water. Baltic Sea ice salinity is lower than that measured in oceanic environment first-year ice. In the northern Baltic, salinities are generally less than 2 psu and even lower (V; Palosuo 1963).

The bulk salinity of the ice varies vertically within the ice cover and the salinity profiles in the Baltic Sea ice quite often do not have the typical C-shaped appearance of polar sea ice (Figure 4). In the Baltic, the highest salinities are usually found in the uppermost parts of the ice cover (Figure 4) presumably due to of rapid growth, flooding, and snow-ice formation, while salinity often tends to decrease towards the bottom (Granskog et al. 2006b). We found that the lower salinities in the bottom layers in part result from lower growth rates (V).

The bulk salinity of sea ice is important for determining the brine volume of sea ice, which is also dependent on temperature. The brine volume can be easily derived from the bulk salinity and temperature measured, using the equations that Cox and Weeks (1983) and Leppäranta and Manninen (1988) formulated. The brine volume is necessary for sea-ice porosity and strength

estimates. The thermodynamic conductivity of ice (Makshtas 1998), ice strength (Timco and O'Brien 1994), ice porosity (Golden et al. 1998), and many aspects of biology (Arrigo 2003) are closely associated with the brine volume of sea ice. The brine volume is a good measure of the habitable space available in the ice; a higher brine volume translates into more and larger habitable spaces in the ice. In the Baltic Sea, ice algal biomass and size of the organisms in the ice increase with increased brine volume (Piiparinen et al. 2010; Piiparinen 2011).

The frazil ice contribution to sea ice can change the salinity profiles in the ice, thus affecting sea-ice strength and ecology, since it typically has higher salinities due to higher numbers of brine pockets than in columnar ice.

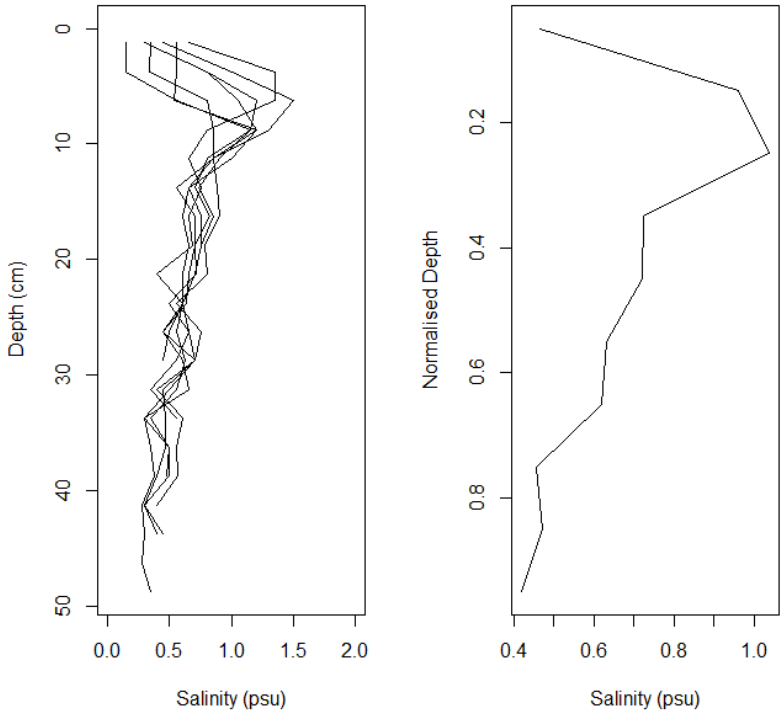

Figure 4. Salinity profiles from Bothnian Bay fast ice, location 3 in Figure 2 (V). Left figure contains salinity profiles from nine cores taken between February 2 and March 15 and right figure shows the composite of these cores with normalized depth profile.

5.1 Parameterizations

Bulk salinity is one of the key characteristics of sea ice, because with it the porosity can be calculated under changing temperature. It is possible to simulate sea-ice growth down to the pore scale and solve brine entrapment with a fine-microstructural ice model (Maus 2009). This is rather time-consuming and impractical, and easier and faster methods are usually used. In most applications, a quasi-steady salinity (also called a stable salinity) is assumed to represent the ice salinities after the initial ice formation when growth conditions are reasonably steady.

To parameterize the quasi-steady salinity in the ice, the concept of an effective salt segregation coefficient (k_{eff}) is often used. In the case of sea ice, the coefficient is simply the ratio of the salinity of sea ice (S_i) to that of parent seawater (S_w) , $S_i = k_{eff}S_w$, and describes the effective partitioning of

solute between the solid and solution. The ice growth rate is closely associated with the segregation coefficient (e.g. Nakawo and Sinha 1981), and this reliably describes the amount of salt in the ice.

We described salt segregation in the growing ice and presented a growth rate to segregation coefficient relationship particularly suited for the Baltic Sea basin with brackish water (V). The relation differs from oceanic relations in that lower sea water salinities change the morphology of the ice-water interface (Figure 5). The Baltic Sea k_{eff} as a function of growth velocity ν_i, for the velocity range $0.2 \cdot 10^{-4} < \nu_i < 4.5 \cdot 10^{-4}$ mm s^{-1} can be described (V) as:

$$k_{eff} = \frac{0.113}{0.113 + 0.887 \exp(-2.66 \times 10^3 \nu_i)} \qquad (10)$$

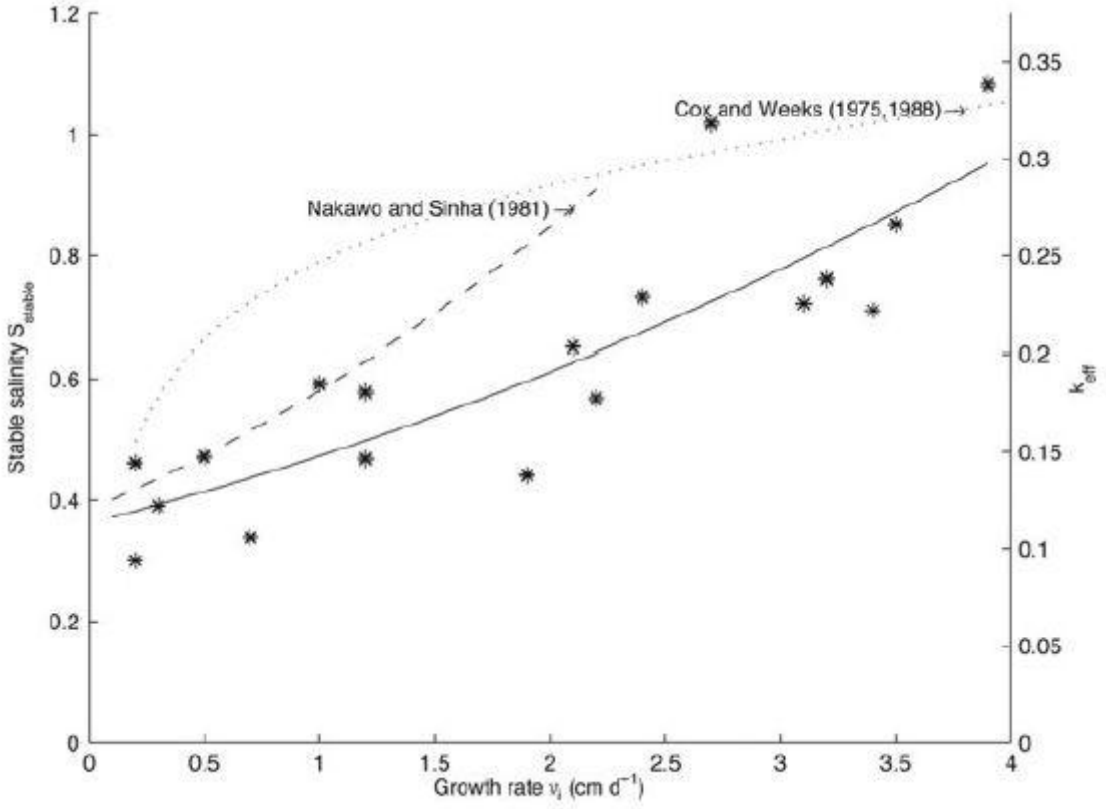

Figure 5. Relationship of stable salinity and effective segregation coefficient (k_{eff}) to growth rate derived from measurements (V) (dots) and using Equation 10 (line). The dashed line shows the corresponding relationship based on Nakawo and Sinha (1981) and the dotted line is based on the Cox and Weeks (1975, 1988) datasets. These relationships are derived from more saline ocean environments.

5.2 Salinity flux between water and ice

We measured salinity transport between the sea ice and underlying seawater in Santala Bay, Sundholm, and Umeå, locations 1A, 1B, and 2, respectively, in Figure 2 (III). The salinity flux was calculated from the conductivity fluxes, using Equation 8. The salinity flux was small in all measurements. Transport was downward during the winter months: between –0.31 x 10^{-7} and –0.40

x 10^{-7} psu m s^{-1}. During the spring melting period, the transport was upwards (average 0.24 x 10^{-7} psu m s^{-1}). This upward transport of salinity could have resulted from a low-salinity surface layer under the ice during the melting period. Under these conditions, the freshwater transport downwards is compensated by the upward flux of saline water from deeper water layers, thus resulting in a salinity flux upwards. Under the leads of the perennial arctic pack ice, the salinity flux was measured between –1.63 x 10^{-6} and –1.54 x 10^{-5} psu m s^{-1} (McPhee and Stanton 1996). The salinity transport in the Baltic Sea is much smaller, mainly because the ice and water salinities are much lower.

The ice-to-water salinity flux creates a more saline and thus denser water layer near the ice bottom. When this layer is denser than the underlying water, density convection occurs and mixes the water layers. In the oceans, this is typically the case, because the water is always denser when colder and more saline. But since the maximum water density in the Baltic Sea is above the freezing point, colder and more saline water is not by definition always heavier and will instigate mixing. Most situations will cause density mixing, but not always, which is demonstrated by the occurrence of supercooled water layers immediately under the ice bottom during our measurements (III).

6 Ice thickness

6.1 Sea-ice thickness distribution

A number of physical processes determine the existence and thickness of the ice cover, the most important of which are those governing the vertical growth and decay of the ice sheet in response to energy fluxes at its upper and lower surfaces (Makshtas 1998). Dynamic processes are also important for ice thickness evolution in the pack ice areas of the Baltic Sea, as well as of the oceans. Ice thermodynamic growth slows down as the ice becomes thicker. Thus ice thicker than fast ice in the pack ice areas is a result of dynamic ice growth. Dynamic ice growth is a result of divergence and convergence inside the ice field driven by wind and water currents.

The first phase of sea-ice cover formation begins when the surface of the ocean cools and an initial ice cover is formed on the surface. This first layer of ice is typically nilas or frazil ice, depending on the roughness of the sea surface. During this stage, sea ice expands in vertical and horizontal space and ice thickness and area increase. The ice thickness is typically quite uniform during this initial ice formation. After the initial ice formation stage, thermodynamic ice growth increases ice thickness, but the ice cover area does not significantly change. During this stage of ice growth, the thickness distribution follows a Gaussian like distribution, which is typical for fast ice areas (Figure 6). This type of distribution results from spatial variations in the marine heat flux and surface properties such as albedo and snow thickness.

Convergent motion in the ice cover causes ice floes to collide, while rafting and stacking of the floes produce thicker ice and ice ridges (Hibler 1979). This changes the ice thickness distribution in the ice field, transforming thinner level ice into thicker deformed ice, but this does not increase the ice volume (Thorndike et al. 1975). Any convergence in the ice field typically results in a contrasting divergent motion. This results in open-water leads where thermodynamic ice growth is more efficient and increases the ice volume more rapidly than in the thicker ice areas (Hibler 1979). In the Baltic Sea area, dynamic processes modify the distribution of ice thickness from fast ice like Gaussian distributions towards multipeaked distributions with large dispersions of pack ice (Leppäranta 1981) (Figure 6). Both deformed and undeformed ice can be divided into several thickness classes. These classes differ in their mechanical and thermodynamic properties (Vihma and Haapala 2009).

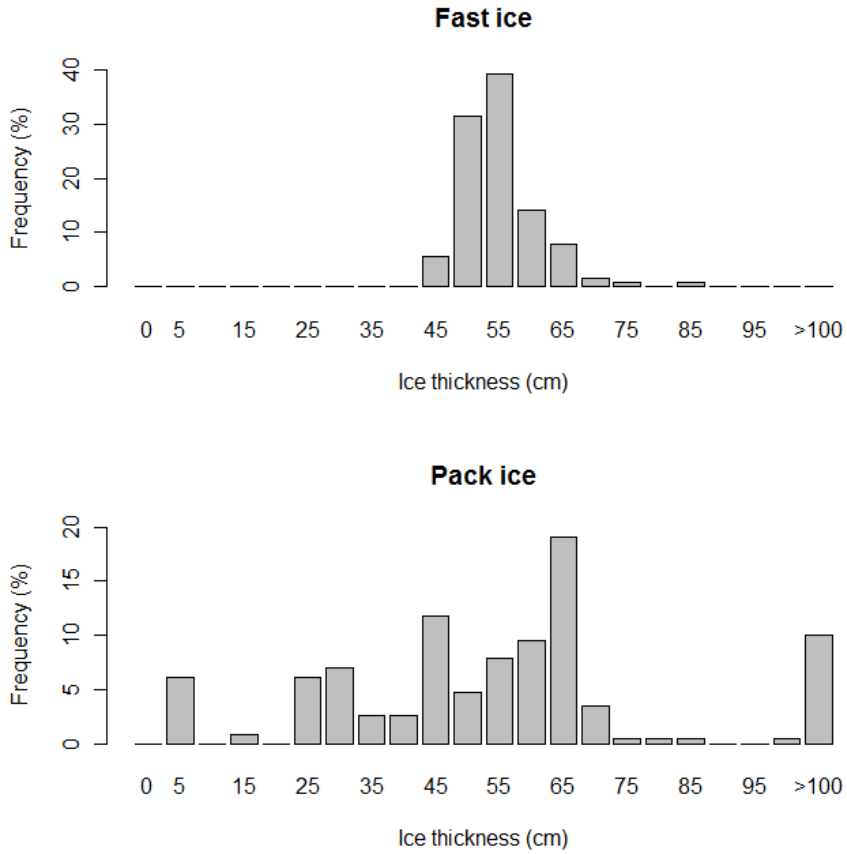

Figure 6. Ice thickness distributions in the Bay of Bothnia, redrawn from Leppäranta (1981). Distribution of ice thicknesses in the fast ice area results from variations in the marine heat flux and surface properties such as albedo and snow thickness, while in the pack ice the distribution is also determined by divergence and convergence in the ice field.

6.2 Thermodynamic growth

The energy flux at the top surface of an ice and snow system is determined largely by the balance of short (SW) and longwave (LW) radiation. SW radiation and surface albedo are the driving factors for the melting sea ice (Perovich 1998). Ice growth is in turn largely controlled by the balance of LW radiation, which can be well estimated by meteorological variables such as air temperature.

The thickness change of ice, *dH/dt*, due to thermodynamic growth or decay at the lower boundary of the ice cover, is determined by the conductive heat flux (F_c) out of the water-ice interface into the ice and the marine heat flux (F_w) from the underlying water. These are balanced by the release or uptake of latent heat (L_{si}) during freezing or melting. The heat budget equation inside the ice is:

$$\frac{d}{dt}(\rho_i c_i T) = \frac{d}{dz}\left(k_i \frac{dT}{dz}\right) - \frac{dF_{SW}}{dz} + \frac{dH}{dt}\rho_i L_{si} - F_W \qquad (11)$$

where ρ_i is ice density, c_i is specific heat of ice, T is ice temperature, k_i is heat conductivity of ice, F_{SW} is net solar SW radiation flux. At the bottom of the ice the energy flux is controlled by heat flux from underlying water. The role of the F_w, as one of the key constituents in the sea-ice energy and mass balance was confirmed in previous studies (Wettlaufer 1991). F_w have been studied quite extensively in arctic and antarctic waters (Petrich and Eicken 2010). These studies have revealed

that local spatial variations in the F_w are small, but influences to the sea-ice thickness and extent are large, suggesting that the ice cover is sensitive to small differences in the local F_w (McPhee et al. 2003).

Under-ice turbulence can result either from mean currents in the water layers under the ice cover or from local convection. Local convection occurs when sea ice grows and the liquid is cooled from above and the rejected salt causes the liquid to become denser. Therefore, both the thermal and the compositional buoyancy have the potential to drive convection (Wettlaufer et al. 1997). However, in this respect the Baltic Sea differs from its oceanic counterpart, because in the brackish water (salinity < 24.7 psu), the temperature of maximum density is reached prior to freezing, further cooling makes the water less dense and therefore there is no thermal convection.

The marine heat flux into the fast ice cover in the Baltic Sea was studied through direct measurements (III) and the maximum 10-minute average heat flux observed during the ice growth period in winter, from water to ice was 18 Wm^{-2} at the Sundholm site, 14 Wm^{-2} at the Umeå site, and 5 Wm^{-2} in Santala Bay. Changes in the F_w correlated with changes in vertical currents. Large negative (downward) F_w values were observed in the Santala Bay region during spring melting and the 10-minute maximum average was -10 Wm^{-2}. In this study, the average F_w was between -0.2 and 1 Wm^{-2} at all sites. Omstedt and Nohr (2004) analyzed a 30-year model simulation for the Baltic Sea and estimated the annual average F_w from water to sea ice to be between 1 and 7 Wm^{-2} for the entire Baltic Sea area. This estimate is slightly larger than ours (III), but Omsted and Nohr's (2004) results included the entire Baltic Sea, not just the coastal fast ice areas we investigated.

In the Arctic Ocean, F_w is typically several Wm^{-2} (Steele and Flato 2000) and in the Antarctic the flux is typically up to several tens of Wm^{-2} (Martinson and Iannuzzi 1998). This comparison shows that F_w in the Baltic Sea is considerably smaller than in the larger oceans. The small F_w values measured in the Baltic Sea may have partially resulted from the presence of lower-density supercooled water layers (0.02 K colder than the freezing point of water) under the ice. Such a layer was observed in the Umeå area during the measurements (III). These periods with supercooled water lasted from one minute to up to two hours. These results suggest that a supercooled and thereby thermally stratified layer may form underneath Baltic Sea ice. Such a layer can limit the convection under the ice and in part explain the small F_w values measured.

The conductive heat flux (F_c) out of the lower boundary is transferred through the ice cover to the upper boundary and ultimately released to the atmosphere. The rate at which this heat exchange occurs at the ice surface is determined by the energy balance at the ice/snow-air interface. For a surface at steady temperature, the conservation of energy requires that the heat fluxes out and into the surface are balanced:

$$(1-\alpha)F_{SW} - I + F_{LW} + H_s + H_l - F_c + F_m = 0 \qquad (12)$$

Here the flux terms are incoming SW radiation flux (F_{SW}) with albedo (α) indicating the ratio of upwelling and downwelling radiation at the surface, the SW flux penetrating through the ice into the water (I), net flux of LW radiation (F_{LW}), the turbulent atmospheric sensible and latent heat fluxes (H_s and H_l), respectively, conductive heat flux from the interior of snow/ice (F_c), heat flux due to melting of ice at the surface (F_m).

Over landfast ice areas, the daily maximum F_{SW} varies from less than 50 Wm^{-2} during midwinter to over 400 Wm^{-2} during the spring melting season. The net effect of SW radiation is then determined by α and I, which are radiative transfer properties of the ice cover and are further considered in the

next chapter. F_{LW} is in most situations directed upwards from the surface and cools the surface. F_{LW} varies typically from 0 to 100 Wm^{-2}, depending on the cloudiness and surface and air temperatures and can in some cases even be downwards, heating the surface (Granskog et al. 2006a; Brümmer et al. 2002). The net radiation flux, combined SW and LW radiations, shows large daily cycles and can vary, depending on the season, from -100 Wm^{-2} (upwards) during freezing conditions to +100 Wm^{-2} (downwards) during the melting season (Granskog et al. 2006a; Brümmer et al. 2002).

H_s and H_l are typically of comparable magnitude and opposite direction, H_s downwards and H_l upwards. Under typical conditions, these are smaller than the net radiation flux, but in cases where advection brings warm air over colder ice surfaces and is accompanied by strong wind, H_s can be much larger than the net radiation flux (Granskog et al. 2006a; Brümmer et al. 2002). However, the surface energy balance on average is determined by the radiation fluxes and is negative during the ice growth season and positive during the melting season. F_m is only relevant during melting periods and is relative to the amount of the melting of ice at the surface. F_c is determined by freezing or melting at the ice bottom, which is also influenced by F_w.

The net effect of surface fluxes on ice cover growth and decay is controlled by the thermophysical properties of ice and snow, of which the thermal conductivity of ice is the most important (Makshtas 1998). The thermal conductivity of any complex material, such as sea ice, is dependent on the thermal conductivities of its components. In the case of sea ice, it consists of crystals of almost freshwater ice, brine, and gaseous bubbles. The thermal conductivity of brine is about one-fourth that of pure ice. The molecular thermal conductivity of gas is smaller by two orders of magnitude. Therefore, ice thermal conductivity decreases as brine volume and porosity increase.

6.2.1 Weather influence on fast ice thickness and properties

Weather conditions largely determine the ice conditions in the landfast ice areas, especially when heat flux from the underlying water is small. We discovered that despite the complexity of processes involved in the growth of the ice cover, the ice thickness and meteoric ice contribution to the ice cover thickness could be explained with basic meteorological variables (I). Thus, it is possible to construct regression models to calculate ice thickness and meteoric ice contribution, using weather observations or climate model results. These models are useful in making estimates of ice thicknesses and meteoric ice contributions in specific areas. The meteoric ice contribution to ice thickness is especially of interest, since it is not currently available from operational ice charts and significantly influences ice optical properties and ice biology.

In Santala Bay, Gulf of Finland, the interannual variations in ice thickness were largely explained by freezing degree days (FDDs) in early winter, December to February (Figure 7a, I). The ice thickness correlated negatively with average winter temperature, precipitation, and wind. Precipitation and wind velocity show strong positive correlation with temperature, because wintertime weather patterns that have high temperatures typically bring more precipitation and higher winds. In this respect, it is reasonable to combine all these correlations to obtain a temperature correlation with ice thickness.

The ice thickness can be estimated with a linear model, using early winter FDD anomaly from an 11-year average that explains 86% of the variability in ice thickness during this period. The difference (residuals) between the linear model and observations was well correlated with wind speed (Figure 7c). Combining the FDD model and wind-speed correction equation resulted in a model that estimated ice thickness very well ($r = 0.993$, p-value < 0.0001) and explained 98% of the

interannual variations in ice thickness from 2001 to 2009. Based on these results, we concluded that the most important weather factors affecting ice thickness are temperature and wind speed. Precipitation does not influence the ice thickness, but is important in determining the ice quality, i.e. the contribution of meteoric ice to the ice thickness.

The contribution of meteoric ice to the annual maximum ice thickness was strongly correlated with the amount of precipitation in early winter; high precipitation resulted in a large contribution of meteoric ice to ice thickness (meteoric contribution = 0.40 * precipitation anomaly + 20.0) (Figure 7b). The snow fraction in the meteoric ice layers was well correlated with wind speed (Figure 7d), but not with precipitation or temperature. Wind affects snow distribution and high wind velocities result in thinner snow cover and steeper temperature gradient in the snow cover, causing more depth hoar formation at the ice-snow interface and less dense snow cover. This in turn decreases the snow fraction in the snow ice layers. Winters with high wind speeds also have thinner layers of meteoric ice. Superimposed ice formation is more likely in years that are colder and wetter than average years.

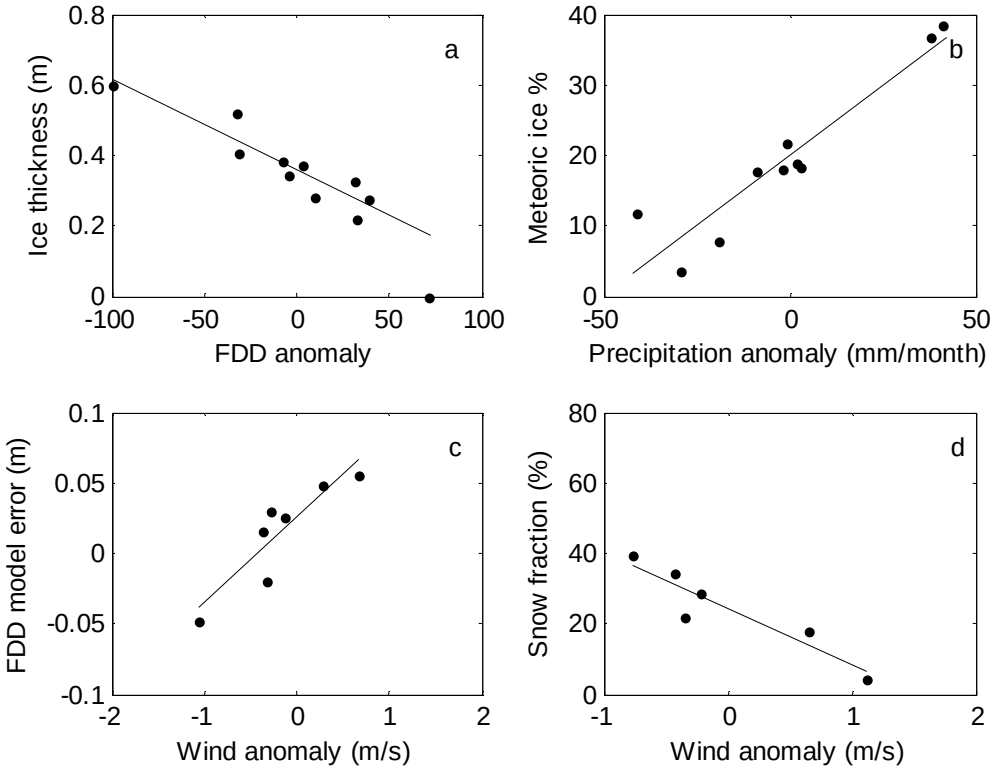

Figure 7. Weather influence on ice thickness and properties in Santala Bay, location 1A, Figure 2: (a) freezing degree day (FDD) anomaly from 11-year early winter mean and winter maximum ice thickness (r = -0.93, p-value 0.0001); (b) early winter precipitation anomaly and meteoric ice contribution to total ice thickness (r = 0.94, p-value = 0.0001); (c) January wind-speed anomaly and total ice thickness error from FDD fit model (r = 0.90, p-value = 0.006); and (d) February wind-speed anomaly and snow fraction of meteoric ice (r = -0.93, p-value = 0.0063). Regression lines are also shown.

7 Radiative transfer in sea ice

The transmittance (*T*) of solar radiation through ice is an important factor affecting biological activity in and under sea ic,e as well as the thermodynamics of the ice cover (Perovich et al. 1993; Perovich 2003). For the ice algal communities in the Bothnian Bay, light is the most important growth-limiting factor (Piiparinen 2011). The most important components controlling the transmission of light through a sea-ice cover are the ice itself, gas and brine inclusions, particulate matter (PM), and colored (also called chromophoric) dissolved organic matter (CDOM) incorporated into the ice cover (Perovich et al. 1998; Belzile et al. 2000). These materials are incorporated into the sea ice during its initial formation from the parent seawater, through flooding of sea ice, or may originate from atmospheric deposition. However, both PM (such as algae) and CDOM produced in ice are also important for the optics of sea ice (Arrigo 2003; Thomas and Papadimitriou 2003). Gas inclusions (e.g. air bubbles) are typically concentrated in the surface-scattering layer and are incorporated in the ice cover through the formation of snow ice or melting and refreezing of the ice surface. The thin-section photographs in Figures 3a and 3b provide some indication of the complexity of the radiative transfer in the ice, since typically the brine and other impurities in the ice cover are concentrated at the crystal boundaries.

Sea-ice albedo (α) is a critical factor for sea-ice energy balance and during the spring melting season the amount of radiation that is absorbed into the ice or transmitted through it, as described by α, largely determines the melting rate of ice. There have been and are numerous efforts to model sea ice and its fate in present and future climates. The α parameterizations are one important but often understated part of the models (Pirazzini et al. 2002; Liu et al. 2007). In an effort to increase the reliability of these parameterizations, all α measurements carried out in Santala Bay were compiled in a sea-ice surface albedo parameterization (VI). This one was notably different from previous parameterizations with respect to detailed handling of the highly scattering surface layers of the ice cover. In this parameterization, the meteoric ice layer thickness significantly contributes to α of bare ice.

7.1 Transmittance

Incident radiation entering the ice can be scattered back to the atmosphere (measured as albedo, α), absorbed within the ice cover, or pass through the ice column. The fate of an individual photon is dependent on the relative contribution of absorption and scattering along its path of travel. Inherent optical properties (IOPs) (absorption coefficient (a) and scattering coefficient (b)) are physical parameters that determine the radiative transfer in the ice with easily defined physical processes behind them. Although these properties are easily understandable, they can be laborious to determine from field measurements and typically require laboratory work before they can be determined. AOPs, such as albedo (α), diffuse attenuation coefficient for downwelling irradiance (K_d), and transmittance (*T*), can be easily measured in the field and are useful in general characterization of the optical properties of sea ice, but are dependent on environmental conditions, such as the angle of incident radiation.

The amount of light passing through the ice cover can be described with spectral transmittance ($T(\lambda)$) as the ratio of downwelling irradiance below the ice cover at depth z ($E_d(z,\lambda)$) to incident downwelling irradiance at the surface $z = 0^+$ ($E_d(0^+,\lambda)$) at a certain wavelength:

$$T(\lambda) = \frac{E_d(z,\lambda)}{E_d(0^+,\lambda)} = e^{-K_d(\lambda)z} \quad (13)$$

When ice is thick enough, an exponential decay of light in the ice can be assumed (Maffione 1998; Maffione et al. 1998). In that case the attenuation of light in the ice can be described with the diffuse attenuation coefficient for downwelling irradiance (K_d), which is wavelength-dependent. K_d describes the amount of irradiance attenuated per meter of material and is also an easy way to compare the radiative properties of different ice layers or covers. Its determination through measurements is relatively straightforward, requiring only simultaneous measurement of irradiance at the top and bottom of the ice cover. K_d is also a very useful indicator of absorption and scattering in the ice. It can be empirically related to *a* (absorption coefficient) and *b* (effective scattering coefficient). Kirk (1991, 1994) formulated this relation as:

$$K_d = \sqrt{a^2 + Gab} \quad (14)$$

where coefficient G is dependent on the shape of the scattering-phase function and varies between 0.233 and 0.264 in natural ice covers.

The high attenuation of radiation in the surface layer shown in Figure 8 is explained by the high scattering coefficient in the surface layer, while temporal changes in the ice cover K_d largely result from changes in surface-layer properties, as was also found in the Arctic Ocean ice cover by Light et al. (2008). Frazil ice layers similarly influence the optical properties of ice through their higher scattering coefficient, due to higher brine volume and smaller crystals.

We observed that the spectral diffuse attenuation coefficient for downwelling irradiance ($K_d(\lambda)$) was lowest at 565 nm in the surface layer, at 560 nm in the columnar layer, and at 575 nm in the under-ice water (Figure 8; II). The shifting of the attenuation minimum between the different ice layers resulted from the difference in CDOM and PM absorption in the layers. The increase in CDOM and PM absorption, with higher absorption at the shorter wavelengths, shifted the minimum attenuation towards longer wavelengths, as was previously observed in the Arctic Ocean ice cover (Perovich et al. 1993; Perovich et al. 1998; Light et al. 2008).

We also observed that the $K_d(\lambda = 565\ \text{nm})$ in the surface layer was between 5.9 and 8.2 m^{-1} and $K_d(\lambda = 325\ \text{nm})$ between 12.0 and 14.4 m^{-1}, while throughout the entire ice cover $K_d(\lambda = 565\ \text{nm})$ was from 1.8 to 2.2 m^{-1} and $K_d(\lambda = 325\ \text{nm})$ from 5.0 to 5.3 m^{-1} (Figure 8; II). The shape and magnitude of K_d for the entire ice cover in our study were very similar to those reported by Ehn et al. (2004) for the Baltic Sea.

We used a radiative transfer model to simulate the effects of CDOM and PM on the transmittance of light through the ice cover (II). We found that CDOM mostly affects the transmission of UV radiation, whereas PM more greatly influences the transmission of PAR (Figure 9; II). The wavelength of maximum transmittance shifted from 580 nm to 548 nm from a high-CDOM to a no-CDOM case. The calculated wavelength of maximum transmittance (562 nm) shifted to 492 nm when PM absorption was removed. Without PM and CDOM, the wavelength of maximum transmittance shifted even further towards UV radiation. A snow layer on the ice strongly influences transmittance, but high absorption by CDOM can have nearly the same influence on the transmittance of UV radiation. This emphasizes the importance of CDOM in UV radiation transmittance in young sea-ice covers.

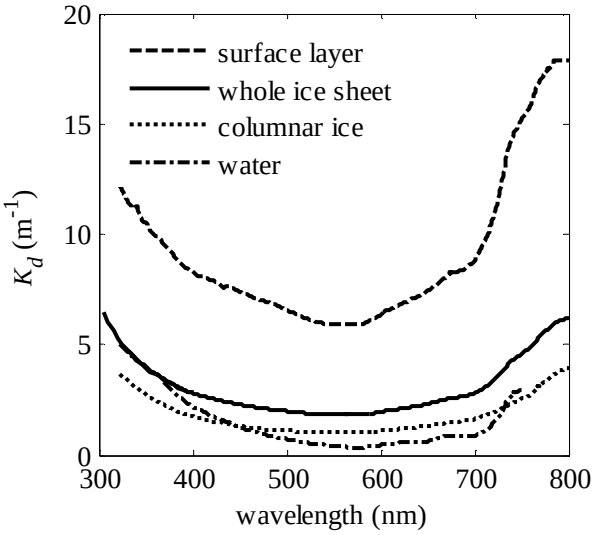

Figure 8. Calculated (surface layer) and measured (whole ice sheet, columnar ice, and water 20 -70 cm below ice bottom) K_d, on 14 March 2007 in Santala Bay (II).

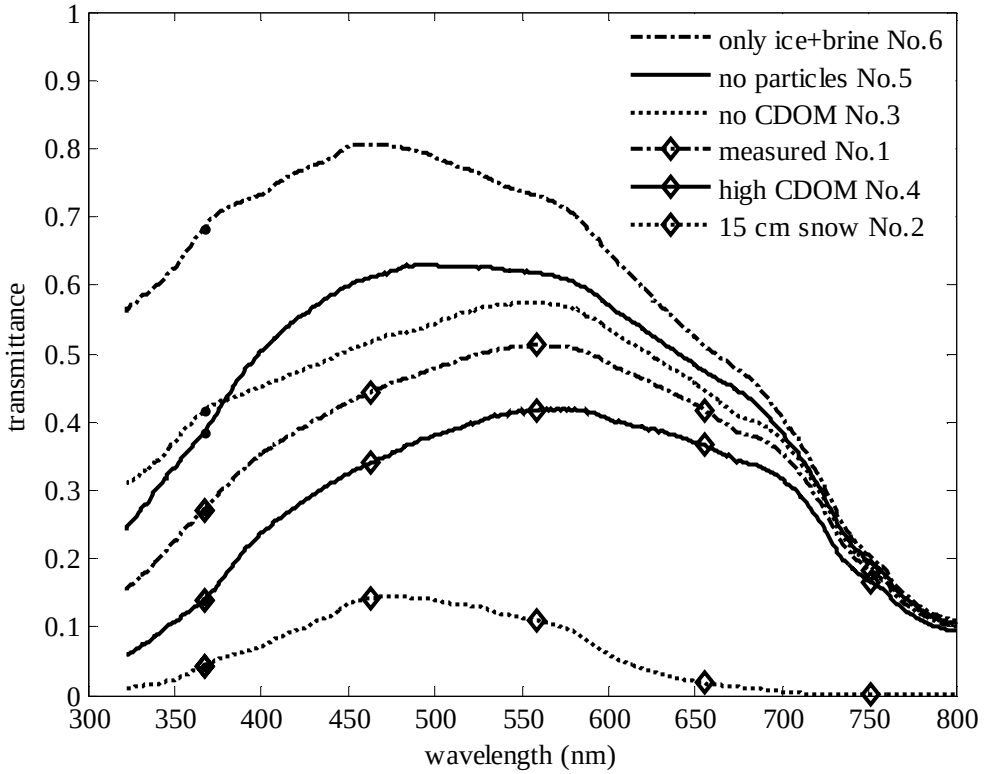

Figure 9. Measured and modeled transmittances for total ice thickness (37 cm thick with 6 cm meteoric ice layer) in Santala Bay, location 1A, Figure 2. The model simulations consisted of different PM and CDOM concentrations in ice and with a 15 cm wet snow layer on top of the ice. A two-way radiation transfer model was used to study the transmittances through the ice cover under six different conditions. The model simulations were 1) the conditions measured, 2) 15 cm wet snow cover on the ice, 3) no CDOM absorption (a_{CDOM} = 0), 4) high CDOM absorption (a_{CDOM} = 0.53 x a_{CDOM} (water)), 5) no PM absorption (a_p = 0), and 6) no CDOM or PM absorption (a_{CDOM} = 0 and a_p = 0).

We observed that CDOM contributed 42%, 36%, 33%, and 20% to the attenuation of radiation in ice at 305 nm, 325 nm, 360 nm, and 550 nm, respectively (II). The importance of CDOM for attenuation increased with depth in the ice cover along with an increase in a_{CDOM} (Figure 14a). In the surface layer, PM and especially mycosporine like amino acids (MAAs) contributed substantially to the attenuation of UV radiation. The absorption and attenuation of UV radiation was mostly controlled by CDOM and PM over the ice and brine. These results show that impurities in ice can have significant implications for ice cover optical properties.

7.2 Albedo

The fraction of the incident irradiance that is reflected back to the atmosphere from the surface is defined as the albedo (α). The spectral albedo ($\alpha(\lambda)$) is defined as the ratio of up- ($E_u(0^+,\lambda)$) to downwelling ($E_d(0^+,\lambda)$) irradiances:

$$\alpha(\lambda) = \frac{E_u(0^+,\lambda)}{E_d(0^+,\lambda)} \quad (15)$$

where λ is the wavelength and 0^+ denotes height immediately above the surface. The total (all-wavelength) albedo (α_t) is the integral over the entire range of solar SW spectrum (commonly taken as 400-1500 nm, Perovich 1998):

$$\alpha_t = \frac{\int E_u(0^+,\lambda)d\lambda}{\int E_d(0^+,\lambda)d\lambda} \quad (16)$$

The α is determined by the combined effect of specular reflection at the surface (typically considered 5% for ice and snow), scattering at the surface, as well as by scattering and absorption in the volume of ice. The α of bare ice surfaces is also strongly dependent on the interior structure of ice. The gas and brine inclusions act as scattering sites in the ice and the α correlates well with the amount of scattering in the ice cover. The amount of gas and brine inclusions per surface area of ice typically correlates with ice thickness and results in an increase in ice α with increase in ice thickness (Petrich and Eicken 2010).

Continuous α measurements from Santala Bay during two winter seasons (2000-2001) enabled us to define representative α values for a multitude of ice thicknesses and surface conditions present in the Baltic Sea landfast ice zone (Table 2). The thickness of the snow cover was the most important factor determining the α. When the snow cover on ice was thin, α values were largely determined by the thickness of snow. The increase in α with the increasing thickness of snow was described by a power function until an average value of 0.90 for thick snow was reached (Figure 10). We concluded that a transition from thin to thick snow cover occurred at a 3.1 cm snow thickness. The age of the snow surface (time from the last new snow) was an important factor for α of thick snow cover, since new (less than two days from last snowfall event) snow-cover α were larger than those of old (two days or more from last snowfall) snow cover (Table 2). Surface temperature (T_s) was also important determinant for the α of thick and old snow cover (Figure 11a). A rise in T_s resulted in a decrease in α at T_s values above -15 ºC, at T_s values below -15 ºC, T_s did not affect the α.

The effect of decreasing α with snow age is also related to the temperature as the speed of snow-ageing processes is related to the temperature. Snow ageing is also caused by the wind when it transports snow crystals from one location to an other and reshapes them. These morphological processes all make the snow crystals smaller and rounder, thus decreasing the reflectance of the crystals. The α of old and thick snow cover on Baltic Sea fast ice (Table 2) is in good agreement with snow α values reported from Antarctica, where snow crystals are typically rounded by wind transport (Rasmus 2006).

The α of bare ice surface was dependent mostly on the thickness of meteoric ice and secondly on surface temperature. Meteoric ice contains numerous air bubbles and consists of small crystals with many small brine inclusions, all of which result in high levels of scattering. Accordingly, an increase in the thickness of the meteoric ice layer results in an increase in scattering and α of bare ice surface. We observed that the relationship of meteoric ice to α was most prominent when meteoric ice was thinner than 3.9 cm (Figure 12a; VI). When the thickness of the meteoric ice layer exceeded 3.9 cm, the α changed due to other effects, such as surface wetness and temperature. Increase in surface temperature or wetness decreased α. The thickness of the meteoric ice layer, after which further increase in thickness did not result in an increase in α, would denote the depth in ice at which all the radiation has been scattered at least once. In this case, increase in the thickness of the scattering layer does not increase the amount of scattered radiation, because all radiation has already been scattered at least once. In this study, a depth of 3.9 cm was that at which almost all the radiation has been scattered at least once. This depth is dependent on the amount of scattering in the ice surface layers and is likely to vary among locations.

The α is highly dependent on the scattering in the surface layer, as noted above (II). Ice freeboard changes significantly influenced the α, because scattering increased with increasing freeboard. This change also significantly influenced the transmittance of the ice cover and K_d. Larger freeboard results in a larger percentage of pores in the ice that are air-filled instead of water-filled. Scattering and hence α is higher from pores filled with air than from those filled with water.

The effect of temperature on the α of bare ice was most prominent in the transition from cold to melting ice (Table 2). When meteoric ice was thicker than 3.9 cm and without any snow cover for at least one day, a rise in temperature resulted in a decrease in the α of bare ice (Figure 11b). Temperature had no effect on the α at temperatures lower than -3 °C. Less than half of the variation in α in bare ice situations with thick (> 3.9 cm) meteoric ice layers was explained with temperature (Figure 11b). Other factors, such as freeboard and meltwater fraction, most likely also contributed significantly to the changes in α.

Changes in total ice thickness of the ice cover also influenced the α, but were mostly overshadowed by changes in meteoric ice layer thickness (Figure 12b). The few days with bare ice cover, i.e. without any meteoric ice, showed increasing α with increasing ice thickness.

Table 2. Representative albedos for various surface types in Santala Bay, location 1A, Figure 2. Calculated from observations, except for thick melting ice with thick snow cover, which was estimated using parameterization equations (VI). The table shows the average albedo ± standard deviation and in parentheses the number of observations in each ice/surface type. T_s is surface temperature.

Ice type	Bare surface (no snow)	Snow < 3.1 cm	Snow ≥ 3.1 cm
Thick ice (≥ 20 cm), all	0.41 ± 0.06 (59)	0.81 ± 0.11 (20)	0.91 ± 0.04 (14)
Thick ice, cold (T_s < -3 °C)	0.47 ± 0.04 (13)	0.85 ± 0.05 (14)	0.90 ± 0.05 (8)
Thick melting ice	0.38 ± 0.05 (24)	0.67 ± 0.15 (4)	0.82*
Thick ice, new snow		0.85 ± 0.17 (13)	0.91 ± 0.04 (11)
Thick ice, old snow		0.80 ± 0.11 (7)	0.84 ± 0.02 (3)
Thin ice (< 20 cm)	0.21 ± 0.11 (27)	0.44 ± 0.31 (9)	0.89 ± 0.06 (6)
Nilas	0.13 ± 0.04 (15)	0.33 ± 0.18 (5)	0.94 ± 0.01 (3)
Open water	0.07 ± 0.01 (30)		

*estimated

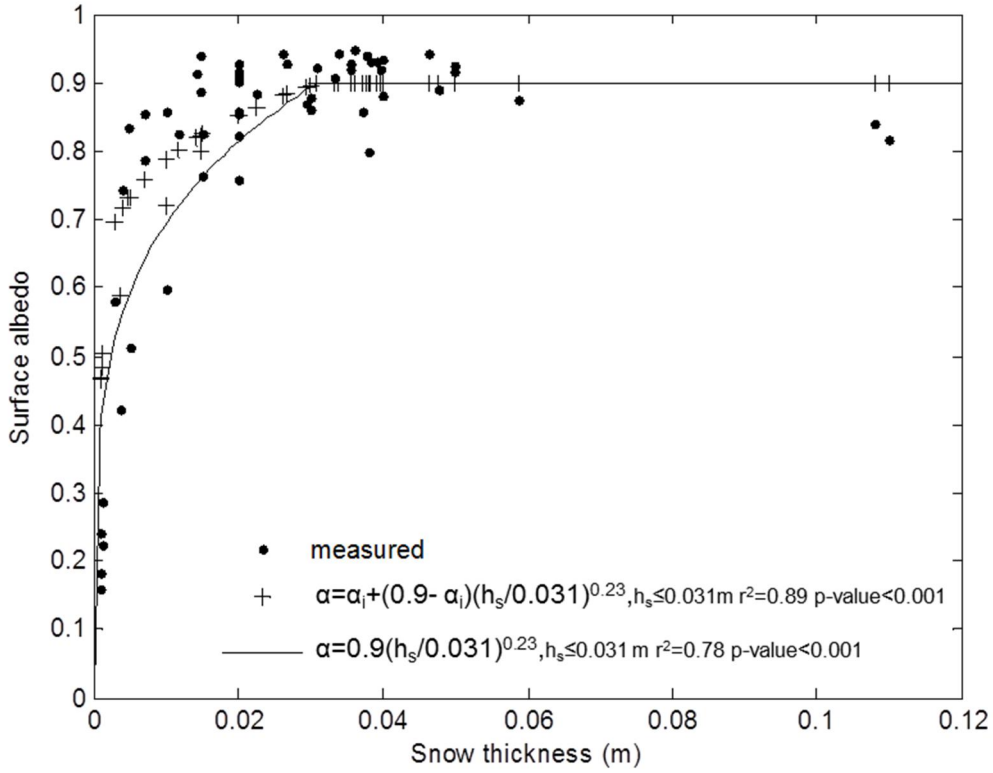

Figure 10. Thickness of snow cover on the ice (h_s) and albedo (α) in Santala Bay, showing measured α, α calculated with parameterization equation (+), where α_i is the α of bare ice, and the best fit to the snow data without information on the underlying ice cover (line).

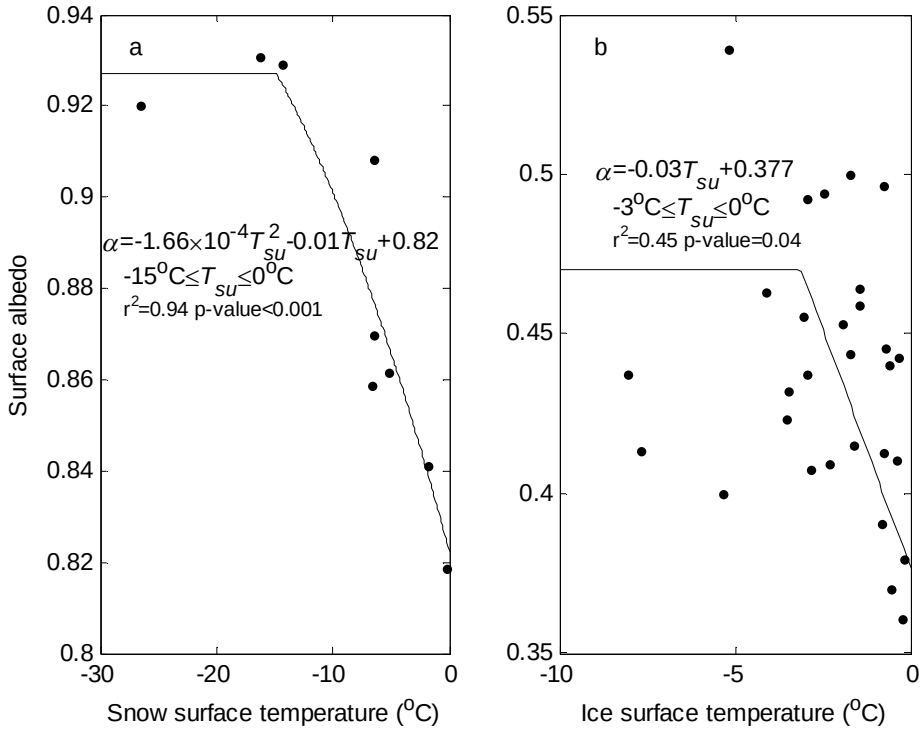

Figure 11. Surface temperature (T_s) and albedo (α) in Santala Bay for (a) snow-covered ice with snow thicker than 3.1 cm and (b) bare ice surface with meteoric ice layer thicker than 3.9 cm.

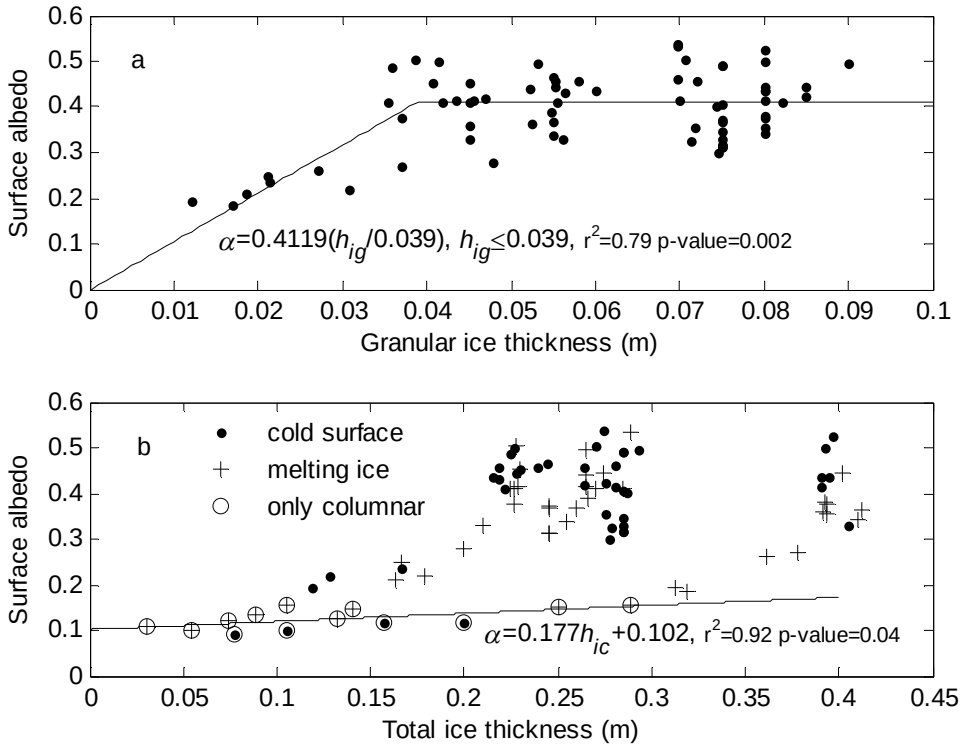

Figure 12. Albedo and (a) granular (meteoric) ice thickness (h_{ig}) during days without snow cover on the ice and (b) total ice thickness during days without snow cover on the ice in Santala Bay. In figure (b) (•) denotes days with dry cold surface and (+) days with wet surface due to rain or melting and if circled ice cover consists of columnar ice only (h_{ic} = columnar ice thickness), i.e. nilas or melting ice with meteoric ice layer already melted away. Shown is the equation of albedo that was fitted to the columnar ice only observations.

7.3 Absorption

The part of irradiance that enters the ice cover and is not scattered back to the atmosphere or transmitted through to the underlying water is absorbed into the ice cover. The total absorption coefficient for sea ice (a_{tot}) can be expressed as the sum of all individual absorbing components that are included in the ice cover: pure ice, brine, and impurities, such as particulate or dissolved matter. Absorption by the air inclusions in sea ice is negligible and were assumed to be zero in ice cover studies (Perovich 1998).

$$\alpha_{tot}(\lambda) = \nu_{pi} a_{pi}(\lambda) + \nu_{br} a_{br}(\lambda) + a_{imp}(\lambda) \qquad (17)$$

where ν denotes the volume fractions of pure ice (*pi*) and brine (*br*), *a* is the absorption coefficient for pure ice (*pi*) and brine (*br*) and a_{imp} is the combined absorption coefficient for all impurities in the ice. The absorption coefficients of ice and brine are wavelength-dependent (Figure 13). Impurities in ice can have a large effect on the absorption in the ice cover. For example, in Santala Bay in the ultraviolet and blue parts of the spectrum, the dissolved and particulate matter absorption coefficients are much larger than a_{pi} or a_{br}.(Figures 13 and 14).

We observed that particulate matter (PM) and colored dissolved organic matter (CDOM) were the largest absorbing components in the ice cover at wavelengths shorter than 600 nm (Figures 13 and

14; II). Above 600 nm, the combined absorption coefficient of ice and brine was the largest. CDOM was the largest single absorber at wavelengths < 380 nm. When the distribution of a_{CDOM} throughout the ice column was examined, we observed that the magnitude of a_{CDOM} was lower and spectrally different in the surface ice layer than in the layers below (Figure 14a). PM was the largest absorbing component throughout the entire ice thickness between 380 nm and 600 nm (Figures 13 and 14) and had the characteristic chlorophyll *a* (Chl *a*) absorption peak at 670 nm (Figure 14b). In addition, a_p was the largest absorbing component in the surface layer and had a distinct peak between 320 nm and 345 nm, with a maximum of 0.73 m^{-1} found at 325 nm (Figure 14b). This peak corresponded to the absorption peak of mycosporine-like amino acids (MAAs), which are a family of photoprotective compounds that have high molar extinction coefficients and therefore absorb UV radiation efficiently. Primary producers synthesize MAAs, which can attenuate UV radiation in the water column (Sommaruga and Psenner 1997; Laurion et al. 2000). The chemical determination of MAAs revealed that they occurred in relatively high concentrations in the ice. The MAAs contribution to the total UV absorption in the ice was 10%, 3%, and 2% of $a_{tot}(\lambda = 325\ nm)$ in the surface, middle, and bottom ice layers, respectively.

The energy of radiation in the UV range is more damaging to organisms per photon absorbed at shorter wavelengths, e.g. at 305 nm, than at 325 nm and the scalar quantum irradiance at 305 nm ($E_{o,q}(\lambda = 305\ nm)$) was two orders of magnitude smaller than $E_{o,q}(\lambda = 325\ nm)$. This could account for the need of microalgae to produce photoprotective substances such as MAAs against UV radiation at 325 nm, rather than protect themselves from potentially more damaging but much less intense shorter wave UV radiation.

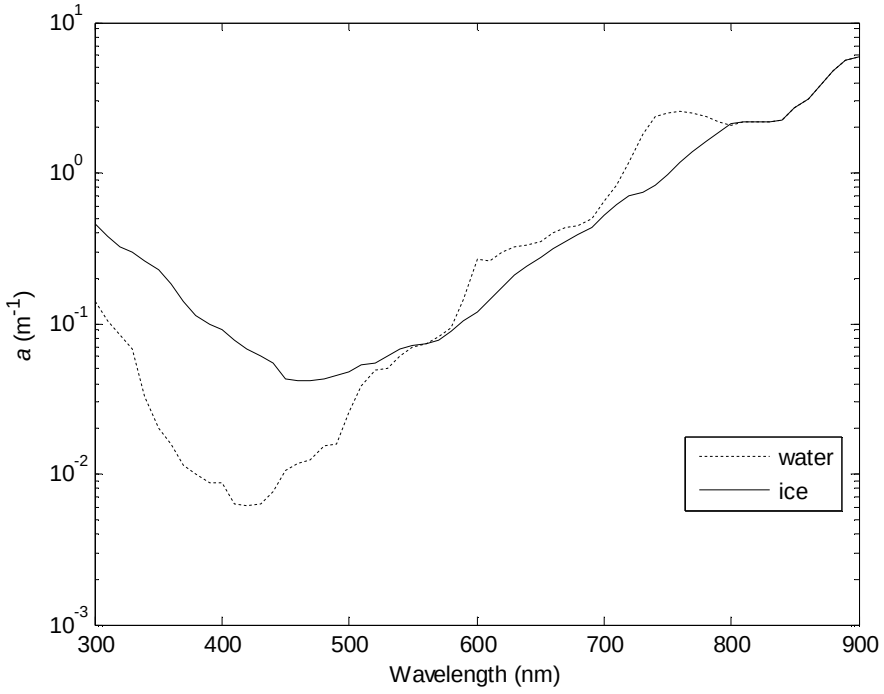

Figure 13. Absorption coefficients of pure ocean water (Smith and Baker 1981; Sogandares and Fry 1997) and ice (Grenfell and Perovich 1981; Perovich and Govoni 1991).

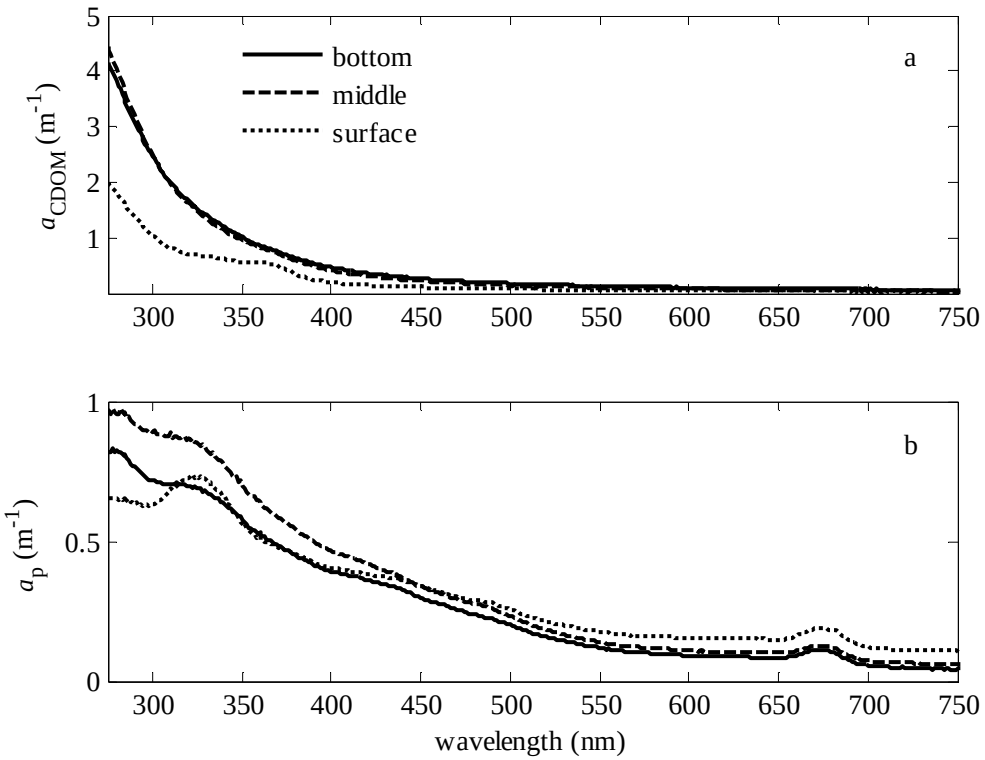

Figure 14. Absorption coefficients in three different ice layers in an ice cover of 37 cm thickness, a) colored dissolved organic matter (CDOM) and b) particulate matter, in Santala Bay (II).

7.4 Scattering

Scattering results from differences in the indices of refraction between ice and the inclusions of particles, liquids, and gas in ice. Gas bubbles are more strongly scattering than brine pockets, because the difference in index of refraction is larger between air (index of refraction = 1) and ice (index of refraction = 1.31) than brine (index of refraction = 1.34) and ice. The index of refraction for brine is temperature-dependent and scattering is larger the colder the brine, because the difference in the indices of refraction between ice and brine become larger (index of refraction = 1.34 at -2 °C and 1.40 at -32 °C, Maykut and Light 1995). The index of refraction for ice, brine, and air at optical wavelengths has very weak wavelength dependence and can be assumed to be constant (Grenfell 1983). When brine becomes colder than -24 °C, solid salts start to form in brine pockets and are much more effective scatterers than liquid brine (Perovich 1998).

Scattering can be defined by two parameters: the scattering coefficient (σ) and phase function (p). The σ is analogous to the absorption coefficient and is a measure of the amount of scattering per unit length. The p describes the angular dependence of scattering and in ice and snow scattering is strongly forward-peaked. These two parameters are combined to form the effective scattering coefficient (b). The b can be assumed to be independent of wavelength, since the scattering elements in sea ice are much larger than the wavelength of light and thus diffraction and interference can be ignored. We estimated that b was 13 m^{-1} in the columnar ice and 430 m^{-1} in the granular ice surface layer (II).

7.5 Light in the ice

The optical (200-2500 nm) band of electromagnetic radiation can be divided into three segments: ultraviolet (UV) radiation from 200 to 400 nm, visible light from 400 to 750 nm, and near-infrared (NIR) from 750 to 2500 nm. The importance of these wavebands to the surface energy budget and biology differ. Visible light and NIR greatly affect the surface energy budget, unlike UV radiation which contributes very little to the total energy of solar radiation. UV radiation can be further divided into UV-A at 315-400 nm, UV-B at 280-315 nm, and UV-C at 200-280 nm. Solar UV-C radiation does not reach the earth's surface. UV-B is largely absorbed by atmospheric ozone, but ozone depletion in the upper atmosphere results in higher UV-B radiation intensities at sea level (Perovich 1998), which could have implications for biology. Due to the high photon energy of UV radiation, it has harmful effects on living cells, such as DNA damage and inhibition of photosynthesis (Arrigo 2003). Various sea-ice algae show different responses to UV-induced damage, such as protection (MAAs) or acclimation. UV-A radiation can shape the species composition and the vertical distribution of Baltic Sea ice algal communities (Piiparinen 2011). Baltic Sea ice algae may also show very slow or no recovery from UV radiation-induced damage (Piiparinen and Kuosa 2011), thus making Baltic Sea ice algae more susceptible to UV radiation than polar ice algae.

We measured the irradiance intensities in Santala Bay (at 12:00 h on 14 March 2007) (II). The downwelling plane quantum irradiance of PAR ($E_{d,PAR}$) was 709 and 351-μmol quanta m^{-2} s^{-1} above and under the ice, respectively. The scalar quantum irradiances ($E_{o,q}$) inside the ice were larger than the $E_{d,q}$ measured as a result of scattering in the ice. For example, $E_{o,PAR}$ at the top of the granular ice layer was 1.6 times larger than the $E_{d,PAR}$ measured above the ice. The $E_{o,PAR}$ measured below the ice exceeded the light-saturating irradiances (app. 150 μmol quanta m^{-2} s^{-1}) for the dominant species of winter phytoplankton in our study region (Spilling 2007), indicating that the light intensities were high for the biological communities in and below the ice. These high PAR intensities can cause photoinhibition and possibly decrease the algal biomass. The mean intensity of UV radiation, $E_{o,q}(\lambda = 325$ nm) for the surface, middle, and bottom layers were 0.31, 0.16, and 0.11 μmol quanta m^{-2} s^{-1}, respectively, and the $E_{d,q}(\lambda = 325$ nm) measured under the ice was 0.06 μmol quanta m^{-2} s^{-1}.

8 Summary

The aim of the studies presented in this thesis was to gain a better understanding of sea-ice physical and optical properties and their influence on the biology of sea ice in the Baltic Sea. The principal results that advanced our knowledge of sea-ice properties were that a) the stratigraphy of the ice and its growth history influenced the vertical distribution of organisms in the ice cover, b) the initial salt entrapment during ice growth in the Baltic Sea was less than in oceans with equal ice growth rates, c) the snow ice contribution of the total ice cover thickness could be estimated using only precipitation data, and d) the turbulent fluxes in the coastal areas were small. The optical studies advanced our knowledge of the ultraviolet radiation properties of ice and organic matter was the most important factor determining these properties, while the albedo of bare sea ice was controlled by the presence and thickness of the meteoric ice layer.

The optical properties of sea ice are crucial to an understanding of the biological environment in the ice and the sea-ice energy budget. The state of the surface meteoric ice layer was the ice property most important to the optical properties of bare ice, whether melting or growing. In previous studies, the influence of meteoric ice on these optical properties has been addressed, but here its effects were for the first time explicitly quantified in the Baltic Sea. The meteoric ice layer, even if only a few centimeters thick, significantly increased the bare ice albedo. This has significant implications for ice-melting progression as well as for the light intensity that organisms encounter in and under the ice. Freeboard height was also an important parameter for ice surface albedo. Despite the crucial influence of freeboard and meteoric ice thicknesses on surface albedo, the snow-cover thickness on the ice was the single most important determinant for the surface albedo. The albedo parameterization presented in this thesis significantly improves the albedo presentation in models describing thin first-year ice. This improved performance is reached because the effect of the highly scattering surface layer of meteoric ice is included in the parameterization. In most large-scale models, the meteoric ice layer thickness is not readily calculated, but this problem can be solved, using accumulated snowfall as a simple estimator of meteoric ice thickness, as demonstrated in this thesis.

The most important factors controlling the transmission of light through the sea-ice cover were identified as the ice itself, gas and brine inclusions, particulate matter (PM), and colored (also called chromophoric) dissolved organic matter (CDOM) incorporated into the ice cover. The organic matter within the sea ice showed significant absorption of UV radiation and modified the UV radiation conditions in and below the ice cover, especially when a snow cover was absent. Organisms in the ice actively altered the UV absorption properties of the ice cover by producing UV-protecting pigments (MAAs) that absorb UV radiation. The significant relationship between the MAA content of a given ice sample and the depth within the ice from which that sample was collected, with the MAA content decreasing with increasing depth, imply that photoprotection by MAAs is crucial to organisms in the ice. These photoprotecting pigments also benefited algae lower in the ice cover or under the ice, since the shading effectively reduced the UV intensities that they received. This is important, because previous studies indicated that ice algae adapted to the low-light conditions prevailing under snow and ice covers are potentially sensitive to UV.

A decade-long time series of ice stratigraphy from a single location demonstrated that sea-ice growth was predominantly determined by air temperature and precipitation. Snow cover on the ice significantly influenced the sea-ice stratigraphy by increasing snow ice growth. Increased precipitation and snow-cover thickness decreased ice thickness and increased only the contribution of snow ice to the total ice thickness. Air temperature did not significantly influence the snow ice

contribution. Snow ice formation also played an essential part in the optical properties of the ice cover, and a simple way to estimate the snow ice contribution was therefore formulated. Increased snow ice contribution and change in the optical properties will probably favor certain sea-ice organisms over other species primarily present in columnar ice.

The sea-ice structure impacted the biological communities in the pack ice zone of the Gulf of Bothnia, and snow ice formation especially seemed to favor certain types of organisms (e.g. centric diatoms). We also recorded that frazil ice production can contribute significantly to ice growth in the Baltic Sea.

The results of this thesis are based on measurements in the Baltic Sea and in relatively thin ice covers. Not all of these results are directly applicable outside of the Baltic Sea area, but since the Arctic Ocean ice cover has become thinner and the area covered by first-year sea ice is increasing, these results could well have significance for the Arctic Ocean as well. The area surrounding Antarctica, which is seasonally ice-covered, is also a suitable area for applying the results obtained in the present study.

8.1 Future scope

Although the present study described the optical properties of sea ice in detail, the applicability of these optical properties may be limited by the temporal and spatial resolution of the measurements. So there is a need to quantify vertical extinction coefficients for different types of ice, i.e. various crystal structure types, salinities, and temperatures. Then we need to consider further how the varying conditions influence the type and magnitude of absorption by particles and dissolved matter. Are our current results of sea-ice optical properties valid for larger areas and longer periods of time?

Information on the optical properties of sea ice could be combined with in situ primary production estimates. Such estimates are already under study by colleagues, at the University of Helsinki, Department of Environmental Sciences, involved as my coauthors in the original publications. Combining the annual sea-ice thickness and type estimates with these optical and primary production results would enable us to calculate annual primary production estimates throughout the sea-ice-covered period. During winter, the ice cover contains more abundant microbial assemblages than the water column. Therefore, the primary producers associated with ice could be capable of taking up more carbon dioxide than the water below. Diminishing ice cover could impact the wintertime CO_2 budget of the Baltic Sea.

It would also be interesting to quantify the importance of irradiance characteristics in the ice to photochemistry. Measuring and modeling the irradiance in ice and measuring the absorption coefficients of light by dissolved organic matter and particulate matter then yields the rates for absorption of radiation. These rates can be converted into photochemical and biological reactions when the apparent quantum yields for these reactions are known.

9 Acknowledgements

Throughout my life I have enjoyed playing with snow and have always been ready to take part in all kinds of snow- and ice-related activities. When starting my academic career, I had already decided to study snow and ice in one form or another. Therefore, I ended up in the field of geophysics and went through all the possible snow, ice, and glacier courses I could get into. So when the possibility to commence PhD studies on sea ice was suggested to me, there was no looking elsewhere. This work was not always easy, but it has given me great experiences and good friends.

First of all, I want to thank Professor Matti Leppäranta, without whose guidance and enthusiasm for ice and snow research I would not have started this PhD work in the first place. During the later phase of the thesis work, Anssi Vähätalo supervised and helped me very generously and I am enormously grateful to him for that.

Mats Granskog helped me through the tougher times every now and then and shared his thoughts when needed. I'm also thankful that he took me along on his research projects. I want to thank Kunio Shirasawa for fruitful cooperation and for the use of his measurement equipment, and I'm sorry that some of them were lost at the bottom of the Baltic Sea. I thank Timo Huttula and Jari Haapala for being much more than their appointment as preexaminers would have required, and helping to improve this thesis considerably. I also thank Anders Omstedt for quick work as an extra preexaminer. I thank James Thompson for reading and improving the language of the thesis.

I am grateful to Jonna Piiparinen for all the fine moments during the fieldwork. I also want to thank her for suggesting that I focus more on the optical studies, which resulted in some of the finest moments during this work. I thank all of my coauthors for all their work and help. Many of the former and some of the present staff at the Division of Geophysics (currently the Division of Geophysics and Astronomy) were of great help in this work by collecting some of the ice samples in Santala Bay and the Bay of Bothnia and also offered some fine company during the coffee breaks and outside of the office. I also want to thank my coworkers at the Department of Environmental Sciences for all the help and company while I had my office in Viikki. I have nothing but praise for all the staff at Tvärminne Zoological Station and Umeå Marine Sciences Center, who facilitated the fieldwork and equipment setup. I also thank my coworkers and superiors at SYKE for their support and good company.

This work was funded by the Walter and Andrée de Nottbeck Foundation, Kone Foundation, Umeå Marine Sciences Center Fund, and the Academy of Finland.

I would not have been able to finish the thesis, even at a snail's pace, without the childcare help that Anni and Kata offered me while on paternal leaves; thank you both!. I'm also very thankful for all the help and support from my dear parents and little brother, without whom this work would not have been possible. The most important support for this work, and in life in general, I received from my dear wife, Jenny. She always motivated me to finish up this work whenever I had a momentary lapse of motivation. Jenny, I love you!

Thank you for reading!

10 References

Arrigo, K. R. 2003. Primary production in sea ice, p. 143-183. *In* D. N. Thomas and G. S. Dieckmann [eds.], Sea ice: An introduction to its physics, chemistry, biology and geology. Blackwell Science.

Belzile, C., S. C. Johannessen, M. Gosselin, S. Demers, and W. L. Miller. 2000. Ultraviolet attenuation by dissolved and particulate constituents of first-year ice during late spring in an Arctic polynya. Limnol. Oceanogr. **45:** 1265-1273.

Brümmer, B., D. Schröder, J. Launiainen, T. Vihma, A.-S. Smedman, and M. Magnusson. 2002. Temporal and spatial variability of surface fluxes over the ice edge zone in the northern Baltic Sea. J. Geophys. Res. **107:** C8,3096, doi:10.1029/2001JC000884.

Cota, G. F., L. Legendre, M. Gosselin, and R. G. Ingram. 1991. Ecology of bottom ice algae: I. Environmental controls and variability. Journal of Marine Systems **2:** 257-277.

Cox, G.F.N. and W.F. Weeks. 1975. Brine drainage and initial salt entrapment in sodium chloride ice. CRREL Res. Rep. 345.

Cox, G. F. N., and W. F. Weeks. 1983. Equations for determining the gas and brine volumes in sea ice samples. J. Glaciol. **29:** 306-316.

Cox, G.F.N. and W.F. Weeks. 1988. Numerical simulations of the profile properties of undeformed first-year sea ice during the growth season. J. Geophys. Res. **93:** (C10) 12,449–12,460.

Curry, J. A., J. L. Schramm, and E. E. Ebert. 1995. Sea ice-albedo climate feedback mechanism. J. Climate **8:** 240-247.

Dieckmann, G. S. , and H. H. Hellmer. 2010. The importance of sea ice: an overview, pp. 1-22. In D. N. Thomas and G. S. Dieckmann [eds.], Sea ice (Second edition). Blackwell Science.

Ehn, J., M. A. Granskog, A. Reinart, and A. Erm. 2004. Optical properties of melting landfast sea ice and underlying seawater in Santala Bay, Gulf of Finland. J. Geophys. Res. **109:** C09003, doi:10.1029/2003JC002042.

Eicken, H. 1998. Deriving modes and rates of ice growth in the Weddell Sea from microstructural, salinity and stable-isotope data. In Jeffries, M.O., ed. Antarctic sea ice: physical processes, interactions and variability. Washington, DC, American Geophysical Union, 89–122. (Antarctic Research Series 74.)

Eicken, H. and M. A. Lange (1989). Development and properties of sea ice in the coastal regime of the southeastern Weddell Sea. J. Geophys. Res. **94:** (C6) 8193-8206.

Feltham, D. L., N. Untersteiner, J. S. Wettlaufer, and M. G. Worster. 2006. Sea ice is a mushy layer. Geophys. Res. Lett. **33:** L14501, doi:10.1029/2006GL026290.

Golden, K. M., S.F. Ackley, and V.I. Lytle. 1998. The percolation phase transition in sea ice. Science **282:** 2238-2241.

Gow, A. J., W. B. Tucker III, and W. F. Weeks. 1987. Physical properties of summer sea ice in the Fram Strait, June-July 1984. CRREL report 87-16: 81 pp., U. S. Army Cold Reg. Res. and Eng. Lab., Hanover, N. H.

Granskog, M. A., T. A. Martma, and R. A. Vaikmäe. 2003. Development, structure and composition of land-fast sea ice in the northern Baltic Sea. J. Glaciol. **49:** 139-148.

Granskog, M. A., M. Leppäranta, T. Kawamura, J. Ehn, and K. Shirasawa. 2004. Seasonal development of the properties and composition of landfast sea ice in the Gulf of Finland, the Baltic Sea. J. Geophys. Res. **109:** C02020, doi:10.1029/2003JC001874.

Granskog, M. A., T. Vihma, R. Pirazzini, and B. Cheng. 2006a. Superimposed ice formation and surface energy fluxes on sea ice during the spring melt-freeze period in the Baltic Sea. J. Glaciol. **52:** 119 -127.

Granskog, M.A., H. Kaartokallio, H. Kuosa, D.N. Thomas, and J. Vainio. 2006b. Sea ice in the Baltic Sea – A review. Estuarine, Coastal and self Science **70:** 145-160.

Granskog, M. A., H. Kaartokallio, and H. Kuosa. 2010. Sea ice in non-polar regions, pp. 531-577. In D. N. Thomas and G. S. Dieckmann [eds.], Sea ice (Second edition). Blackwell Science.

Grenfell, T.C. 1983. A theoretical model of the optical properties of sea ice in the visible and near infrared. J. Geophys. Res. **88:** 9723-9735.

Grenfell, T. C., and D. K. Perovich. 1981. Radiation absorption-coefficients of polycrystalline ice from 400-1400 nm. J. Geophys. Res. **86:** 7447-7450.

Grenfell, T. C., B. Light, and D. K. Perovich. 2006. Spectral transmission and implications for the partitioning of shortwave radiation in arctic sea ice. Ann. Glaciol. **44:** 1-6, doi:10.3189/172756406781811763.

Haas, C., D. N. Thomas, and J. Bareiss. 2001. Surface properties and processes of perennial Antarctic sea ice in summer. Journal of Glaciology **47:** 613-625.

Hibler III, W. D. 1979. A dynamic-thermodynamic sea ice model. J. Phys. Oceanogr. **9:** 815-846.

Hobbs, P. 1974. Ice physics. Oxford University Press, 837 pp.

Holland, M. M., C. M. Bitz, and A. J. Weaver. 2001. The influence of sea ice physics on simulations of climate change. J. Geophys. Res. **106:** (C9) 19639-19655.

Holland, M. M., and C. M. Bitz. 2003. Polar amplification of climate change in coupled models. Climate Dyn. **21:** 221-232.

Jeffries, M. O., R. A. Shaw, K. Morris, A. L. Veazey, and H. R. Krouse. 1994. Crystal structure, stable isotopes ($\delta^{18}O$), and development of sea ice in the Ross, Amundsen, and Bellinghausen seas, Antarctica. J. Geophys. Res. **99:** 985-995.

Jeffries, M. O., A. P. Worby, K. Morris, and W. F. Weeks. 1997. Seasonal variations in the properties and structural composition of sea ice and snow cover in the Bellingshausen and Amundsen Seas, Antarctica. J. Glaciol. **43:** 138-151.

Kaartokallio, H. 2004. Food web components, and physical and chemical properties of Baltic Sea ice. Mar. Ecol. Progr. Ser. **273**: 49–63.

Kawamura, T., K. Shirasawa, N. Ishikawa, A. Lindfors, K. Rasmus, M. A. Granskog, J. Ehn, M. Leppäranta, T. Martma, and R. Vaikmae. 2001. Time-series observations of the structure and properties of brackish ice in the Gulf of Finland. Ann. Glaciol. **33:** 1-4.

Kirk, J. T. O. 1991. Volume scattering function, average cosines, and the underwater light-field. Limnol. Oceanogr. **36:** 455-467.

Kirk, J. T. O. 1994. Characteristics of the light-field in highly turbid waters - a Monte-Carlo study. Limnol. Oceanogr. **39:** 702-706.

Lange, M. A., P. Schlosser, S. F. Ackley, P. Wadhams, and G. S. Dieckmann .1990. ^{18}O concentrations in sea ice of the Weddell Sea, Antarctica. J. Glaciol. **36:** 315-323.

Laurion, I., M. Ventura, J. Catalan, R. Psenner, and R. Sommaruga. 2000. Attenuation of ultraviolet radiation in mountain lakes: Factors controlling the among- and within-lake variability. Limnol. Oceanogr. **45:** 1274-1288.

Leppäranta, M. 1981. On the structure and mechanics of pack ice in the Bothnian Bay. Finnish Marine Research **248:** 3-86

Leppäranta, M., and T. Manninen. 1988. The brine and gas content of sea ice with attention to low salinities and high temperatures. Finnish Inst. Marine Res. Internal Rep. **88-2**, Helsinki.

Leppäranta, M., L. Makkonen, E. Palosuo, and E. Kuusisto. 2001. Geophysics of snow and ice in Finland during the 1900s. Geophysica **37**: 261–285.

Leppäranta, M., and K. Myrberg. 2009. Physical oceanography of the Baltic Sea. Springer-Praxis books in geophysical sciences.

Light, B., T. C. Grenfell, and D. K. Perovich. 2008. Transmission and absorption of solar radiation by Arctic sea ice during the melt season. J. Geophys. Res. **113:** C03023, doi:10.1029/2006JC003977.

Liu, J., Z. Zhang, J. Inoue, and R. M. Horton. 2007. Evaluation of snow/ice albedo parameterizations and their impacts on sea ice simulation. Int. J. Climatol. **27:** 81-91.

Maffione, R. A. 1998. Theoretical developments on the optical properties of highly turbid waters and sea ice. Limnol. Oceanogr. **43:** 29-33.

Maffione, R. A., J. M. Voss, and C. D. Mobley. 1998. Theory and measurements of the complete beam spread function of sea ice. Limnol. Oceanogr. **43:** 34-43.

Makshtas, A. P. 1998. Thermodynamics of sea ice, p. 289-304. In M. Leppäranta [eds.], Physics of ice-covered seas, Vol. 1. Helsinki University Press, Helsinki, Finland.

Martinson, D. G., and R. A. Iannuzzi. 1998. Antarctic Ocean-Ice Interaction: Implications from Ocean Bulk Property Distributions in the Weddell Gyre, p. 243-271. In M. Jeffries [eds.], Antarctic Research Series, Antarctic Sea Ice: Physical Processes, Interactions and Variability. American Geophysical Union, Boston.

Maus, S. 2009. On geophysical property modeling of sea ice: microstructure and salinity. Proceedings of the 6th workshop on Baltic Sea ice climate. Report Series in Geophysics **61**, University of Helsinki: 99-112.

Maykut, G. A., and T. C. Grenfell. 1975. The spectral distribution of light beneath first-year sea ice in the Arctic Ocean. Limnol. Oceanogr. **20**(4): 554-563.

Maykut, G.A., and B. Light. 1995. Refractive index measurements in freezing sea ice and sodium chloride brines. Appl. Optics **34:** 950-961.

McPhee, M.G. 1992. Turbulent heat flux in the upper ocean under sea ice. J. Geophys. Res. **97:** (C4) 5365-5379.

McPhee, M.G. 2002. Turbulent stress at the ice/ocean interface and bottom surface hydraulic roughness during the SHEBA drift. J. Geophys. Res. **107:** (C10) 8037, doi:10.1029/2000JC000633.

McPhee, M.G. and T.P. Stanton. 1996. Turbulence in the statically unstable oceanic boundary layer under Arctic leads. J. Geophys. Res. **101:** (C3) 6409-6428.

McPhee, M.G., T. Kikuchi, J.H. Morison and T.P. Stanton. 2003. Ocean-to-ice heat flux at the North Pole environmental observatory. Geophys. Res. Lett. **30:** 2274, doi:10.1029/2003GL018580.

Mock, T., and D. N. Thomas. 2005. Recent advances in sea-ice microbiology. Environ. Microbiol. **7:** 605-619.

Nakawo, M., and N.K. Sinha. 1981. Growth rate and salinity profile of first-year sea ice in the High Arctic. J. Glaciol. **27:** 315–330.

Omstedt, A. 1985. An investigations of the crystal structure of sea ice in the Bothnian Bay. SMHI RHO **40:** 1-19.

Omstedt, A., and C. Nohr. 2004. calculating the water and heat balances of the Baltic Sea using ocean modeling and available meteorological, hydrological and ocean data. Tellus **56A:** 400-414.

Palosuo, E. 1961. Crystal structure of brackish and fresh-water ice. Int. Assoc. Sci. Hydrology **54:** 9-14.

Palosuo, E. 1963. The Gulf of Bothnia in winter. II. Freezing and ice forms. Merentutkimuslaitoksen Julkaisu/Havsforskningsinst. Skr. **209:** 42-64.

Perovich, D. K. 1998. The optical properties of sea ice, p. 195-230. In M. Leppäranta [eds.], Physics of ice-covered seas. Helsinki University Press.

Perovich, D. K. 2003. Complex yet translucent: The optical properties of sea ice. Physica B **338:** 107-114.

Perovich, D. K., and J. W. Govoni. 1991. Absorption-coefficients of ice from 250 to 400 nm. Geophys. Res. Lett. **18:** 1233-1235.

Perovich, D. K., G. F. Cota, G. A. Maykut, and T. C. Grenfell. 1993. Bio-optical observations of first-year Arctic sea-ice. Geophys. Res. Lett. **20:** 1059-1062.

Perovich, D. K., C. S. Roesler, and W. S. Pegau. 1998. Variability in Arctic sea ice optical properties. J. Geophys. Res. **103:** 1193-1208.

Petrich, C., and H. Eicken. 2010. Growth, structure and properties of sea ice, p. 23-77. *In* D. N. Thomas and G. S. Dieckmann [eds.], Sea ice (Second edition). Blackwell Science.

Piiparinen, J. 2011. Fast- and drift-ice communities in the Bothnian Bay and the impact of UVA radiation on the Baltic Sea ice ecology. Walter and Andrée de Nottbeck Foundation Scientific Reports **36:** 1-57.

Piiparinen, J., H. Kuosa, and J.-M. Rintala. 2010. Winter-time ecology in Bothnian Bay, Baltic Sea: Nutrients algae in fast-ice. Polar Biol. **33:** 1445-1461.

Piiparinen, J., and H. Kuosa. 2011. Impact of UVA radiation on algae and bacteria in Baltic Sea ice. Aquat. Microb. Ecol. **63:** 75-87.

Pirazzini, R., T. Vihma, J. Launiainen, and P. Tisler. 2002. Validation of HIRLAM boundary-layer structures over the Baltic Sea. Boreal Env. Res. **7:** 211-218.

Prezelin, B. B., M. A. Moline, and H. A. Matlick. 1998. Icecolors '93: Spectral UV radiation effects on Antarctic frazil ice algae, p. 45-83. In M. Lizotte and K. Arrigo [eds.], Antarctic sea ice: Biological process, interactions, and variability. Antarctic Research Series, AGU.

Rasmus, K. 2006. Field measurements of the total and spectral albedo of snow and ice in Dronning Maud Land, Antarctica. Geophysica **42:** 17-34.

Rasmus, K., J. Ehn, A. Reinart, M. Granskog, E. Kärkäs, M. Leppäranta, A. Lindfors, A. Pelkonen, and S. Rasmus. 2002. Optical measurements of sea ice in the Gulf of Finland. Nordic Hydrology **33:** 207-226.

Rind, D., R. Healy, C. Parkinson, and D. Martinson. 1995. The role of sea ice in 2 x CO_2 climate model sensitivity. Part I: The total influence of sea ice thickness and extent. J. Climate **8:** 449-463.

Shirasawa, K. and R.G. Ingram. 1991a. Characteristics of the turbulent oceanic boundary layer under sea ice. Part 1: A review of the ice-ocean boundary layer. J. Mar. Syst. **2:** 153-160.

Shirasawa, K. and R.G. Ingram. 1991b. Characteristics of the turbulent oceanic boundary layer under sea ice. Part 2: Measurements in southeast Hudson Bay. J. Mar. Syst. **2:** 161-169.

Smith, R. C., and K. S. Baker. 1981. Optical properties of the clearest natural-waters (200-800 nm). Appl. Opt. **20:** 177-184.

Sogandares, F. M., and E. S. Fry. 1997. Absorption spectrum (340-640 nm) of pure water. I. Photothermal measurements. Appl. Opt. **36:** 8699-8709.

Sommaruga, R., and R. Psenner. 1997. Ultraviolet radiation in a high mountain lake of the Austrian Alps: air and underwater measurements. Photochem. Photobiol. **65:** 957-963.

Spilling, K. 2007. Dense sub-ice bloom of dinoflagellates in the Baltic Sea, potentially limited by high pH. J. Plankton Res. **29:** 895-901.

Steele, M., and G. M. Flato. 2000. Sea ice growth, melt, and modeling: a survey, p. 549-587. *In* E. L. Lewis [eds.], The freshwater budget of the Arctic Ocean. Kluwer Academic Publishers, Dordrescht.

Tassan, S., and G. M. Ferrari. 2002. A sensitivity analysis of the 'Transmittance-Reflectance' method for measuring light absorption by aquatic particles. J. Plankton Res. **24:** 757-774.

Thomas, D. N., and S. Papadimitriou. 2003. Biogeochemistry of sea ice, p. 267-302. In D. N. Thomas and G. S. Dieckmann [eds.], Sea ice: An introduction to its physics, chemistry, biology and geology. Blackwell Science.

Thorndike, A. S., D. A. Rothrock, G. A. Maykut, and R. Colony. 1975. The thickness distribution of sea ice. J. Geophys. Res. **80:** 4501-4513.

Timco, G. W., and S. O'Brien. 1994. Flexural strength equation for sea ice. Cold Reg. Sci. Technol. **22:** 285-298.

Tison, J.-L., A. Khazendar, and E. Roulin. 2001. A two-phase approach to the simulation of the combined isotope/salinity signal of marine ice. J. Geophys. Res. **106:** 31387-31401.

Toyota, T., T. Kawamura, K. I. Ohshima, H. Shimoda, and M. Wakatsuchi. 2004. Thickness distribution, texture and stratigraphy, and a simple probabilistic model for dynamical thickening of sea ice in the southern Sea of Okhotsk. J. Geophys. Res. **109:** C06001, doi:10.1029/2003JC002090.

Vihma, T., and J. Haapala. 2009. Geophysics of sea ice in the Baltic Sea: A review. Progress in Oceanography **80:** 129-148.

Week, W.F. 1998. On the history of research on sea ice, p. 1-24. In M. Leppäranta [eds.], Physics of Ice-Covered Seas, Vol. 1. University of Helsinki Press, Helsinki, Finland.

Weeks, W. F., and S. F. Ackley. 1982. The growth, structure, and properties of sea ice. CRREL Monogr. 82-1.

Weeks, W. F., A. J. Gow, P. Kosloff, and S. Digby-Argus. 1990. The internal structure, composition and properties of brackish ice from the Bay of Bothnia. CRREL Monogr. 90-1: 5-15.

Wettlaufer, J. S. 1991. Heat flux at the ice-ocean interface. J. Geophys. Res. **96:** (C4) 7215-7236.

Wettlaufer, J. S., M. G. Worster and H. E. Huppert. 1997. Natural convection during solidification of an alloy from above with application to the evolution of sea ice. J. Fluid Mech. **344**:

WMO. 1970. WMO sea-ice nomenclature, terminology, codes and illustrated glossary. WMO/ OMM/ BMO, Geneva,World Meteorological Organisation.